

CHARACTERIZATION OF THE MOH1 PROTEIN IN THE YEAST MODEL

A THESIS SUBMITTED TO  
THE GRADUATE SCHOOL OF NATURAL AND APPLIED SCIENCES  
OF  
MIDDLE EAST TECHNICAL UNIVERSITY

BY

ÇAĞLA ECE OLGUN

IN PARTIAL FULFILLMENT OF THE REQUIREMENTS  
FOR  
THE DEGREE OF DOCTOR OF PHILOSOPHY  
IN  
MOLECULAR BIOLOGY AND GENETICS

AUGUST 2024



Approval of the thesis:

**CHARACTERIZATION OF THE MOH1 PROTEIN IN THE YEAST  
MODEL**

submitted by **ÇAĞLA ECE OLGUN** in partial fulfillment of the requirements for  
the degree of **Doctor of Philosophy in Molecular Biology and Genetics, Middle  
East Technical University** by,

Prof. Dr. Naci Emre Altun  
Dean, **Graduate School of Natural and Applied Sciences** \_\_\_\_\_

Prof. Dr. Mesut Muyan  
Head of the Department, **Biological Sciences** \_\_\_\_\_

Prof. Dr. Mesut Muyan  
Supervisor, **Biological Sciences, METU** \_\_\_\_\_

**Examining Committee Members:**

Prof. Dr. Ayşe Elif Erson Bengan  
Biological Sciences, METU \_\_\_\_\_

Prof. Dr. Mesut Muyan  
Biological Sciences, METU \_\_\_\_\_

Assoc. Prof. Dr. Nurcan Tunçbağ  
Chemical and Biological Engineering, Koç University \_\_\_\_\_

Assoc. Prof. Dr. Erkan Kiriş  
Biological Sciences, METU \_\_\_\_\_

Prof. Dr. Demet Çetin  
Mathematics and Science Education, Gazi University \_\_\_\_\_

Date: 29.08.2024

**I hereby declare that all information in this document has been obtained and presented in accordance with academic rules and ethical conduct. I also declare that, as required by these rules and conduct, I have fully cited and referenced all material and results that are not original to this work.**

Name Last name: Çaęla Ece Olgun

Signature:

## ABSTRACT

### CHARACTERIZATION OF THE MOH1 PROTEIN IN THE YEAST MODEL

Olgun, Çağla Ece  
Doctor of Philosophy, Molecular Biology and Genetics  
Supervisor: Prof. Dr. Mesut Muyan

August 2024, 84 pages

The primary circulating estrogen hormone, 17 $\beta$ -estradiol (E2), plays important roles in the physiology and pathophysiology of many tissues. The regulation of cell functions in tissues in response to E2 is mediated primarily by estrogen receptor (ER) alpha, a transcription factor. Identifying E2-responsive genes and protein products could be critical for developing prognostic tools or therapeutic targets.

Our previous studies revealed that *YPEL2* is an estrogen-responsive gene, which is a member of a YPEL family, *YPEL1- YPEL5*, with highly conserved sequence homology encoding YPEL proteins with similar structural and functional features. This similarity renders deciphering the functional features of *YPEL2* in the presence of other YPELs difficult. Nevertheless, using an inducible expression system we showed that *YPEL2* interacts with proteins involved in oxidative stress. However, the mechanism by which *YPEL2* exerts its effects is unclear. In yeast, there is one *YPEL* homolog: *MOH1*. This provides an opportunity to analyze *YPEL2* functions independently of YPELs using yeast complementation approaches. Although mechanisms are unknown, my MSc studies on Moh1p functions suggested that *MOH1* contributes to stress responses affecting cell survival.

In this study, I aimed to attribute functions to Moh1p using the *MOH1*-deleted yeast strain, *moh1 $\Delta$* , and assess its effect on cell morphology, biomolecular composition,

and transcriptomic profile. Our scanning electron microscopy studies indicate structural alterations in the cell wall of moh1 $\Delta$ . Fourier Transform Infrared Spectroscopy and RNA sequencing reveal dramatic lipid and protein modifications resulting from differentially expressed genes that encode proteins involved in lipid and protein metabolisms and stress responses.

Keywords: MOH1, *S. Cerevisiae*, FT-IR, RNA-Sequencing, Scanning Electron Microscopy

## ÖZ

### MOH1 PROTEİNİNİN MAYA MODELİNDE KARAKTERİZASYONU

Olgun, Çağla Ece  
Doktora, Moleküler Biyoloji ve Genetik  
Tez Yöneticisi: Prof. Dr. Mesut Muyan

Ağustos 2024, 84 sayfa

Dolaşımdaki birincil östrojen hormonu olan 17 $\beta$ -östradiol (E2), birçok dokunun fizyolojisi ve patofizyolojisinde önemli roller oynar. Dokulardaki hücre fonksiyonlarının E2'ye yanıt olarak düzenlenmesi birincil olarak bir transkripsiyon faktörü olan östrojen reseptör (ER) alfa tarafından gerçekleştirilir. E2'ye Duyarlı genlerin ve protein ürünlerinin belirlenmesi, prognostik araçların veya terapötik hedeflerin geliştirilmesi için kritik öneme sahip olabilir.

Önceki çalışmalarımız, *YPEL2*'nin östrojene duyarlı bir gen olduğunu ortaya çıkarmıştır. *YPEL2*, benzer yapısal ve fonksiyonel özelliklere sahip *YPEL* proteinlerini (*YPEL1* – *YPEL5*) kodlayan yüksek oranda korunmuş sekans homolojisine sahip, *YPEL* ailesinin bir üyesidir. Bu benzerlik, diğer *YPEL*'lerin varlığında *YPEL2*'nin işlevsel özelliklerinin tayin edilmesini zorlaştırmaktadır. Buna rağmen, indüklenebilir bir ekspresyon sistemi kullanarak *YPEL2*'nin oksidatif strese dahil olan proteinlerle etkileşime girdiğini gösterdik. Ancak *YPEL2*'nin etkilerini hangi mekanizma üzerinden gerçekleştirdiği belirsizdir. Mayadaki tek *YPEL* homoloğu *MOH1*'dir. Bu, maya tamamlama yaklaşımlarını kullanarak *YPEL2* fonksiyonlarını *YPEL*'lerden bağımsız olarak analiz etme fırsatı sağlar. *Moh1p*'nin fonksiyonları üzerine gerçekleştirdiğim yüksek lisans çalışmalarım, mekanizmaları bilinmemekle birlikte, *MOH1*'in hücrenin strese tepkisine katkıda bulunarak hücrenin hayatta kalmasını etkilediğini önermektedir.

Bu çalışmada, *MOH1* silinmiş maya suşu *moh1Δ*'yi kullanarak *Moh1p*'ye fonksiyonlar atfetmeyi ve *Moh1p*'nin hücre morfolojisi, biyomoleküler kompozisyon ve transkriptomik profil üzerindeki etkisini değerlendirmeyi amaçladım. Taramalı elektron mikroskobu çalışmalarımız *moh1Δ*'nin hücre duvarındaki yapısal değişiklikleri göstermektedir. Fourier Dönüşümü Kızılötesi Spektroskopisi ve RNA sekanslama çalışmalarımız, lipid ve protein metabolizmalarında ve stres yanıtlarında yer alan proteinleri kodlayan genlerin ifadesindeki değişikliklerden kaynaklanan dramatik lipid ve protein modifikasyonlarını ortaya koymaktadır.

Anahtar Kelimeler: *MOH1*, *S. Cerevisiae*, FT-IR, RNA-Sequencing, Taramalı Elektron Mikroskobu

To my late grandmother, whose perseverance in life has always been an inspiration

## ACKNOWLEDGMENTS

I would like to thank my advisor, Prof. Dr. Mesut Muyan, for his unwavering support and encouragement throughout my PhD studies. Dr. Muyan provided scientific guidance, through which I learned to think critically, conduct research independently, and plan future steps.

I would like to thank all my thesis committee members, Prof. Dr. Ayşe Elif Erson Bensen, Assoc. Prof. Nurcan Tunçbağ, Prof. Dr. Demet Çetin and Assoc. Prof. Erkan Kiriş for their time and their critical feedbacks.

I specifically express my gratitude to Prof. Dr. Zekiye Suludere and Prof. Dr. Demet Çetin who enabled and conducted scanning electron microscopy. I also sincerely thank to Assistant Prof. Dr. Nihal Şimşek Özek for carrying out FTIR analyses. I would like to thank you Asst. Prof. Nihal Terzi Çizmecioglu, Prof. Dr. Mark Dumont, Prof. Dr. Ahmet Koç, and Prof. Dr. Devrim Çağdaş Son for their valuable suggestions and helpful discussions on my studies.

I want to express my gratitude to my past and current labmates, Gizem G p r, Pelin Yaşar, Gamze Ayaz Şen, Gizem Kars, Burcu Karakaya, Kerim Yavuz, Gizem Turan, Hazal Ayten, Pelin Toker, and B şra Bınarcı for their support, both morally and experimentally. I am also grateful to my dearest lifelong friends, Gizem Kars, Burcu Karakaya, Kerim Yavuz, and Ayşeg l  zman, for never leaving me alone and always making me feel their support from different continents.

I don't know how to express my gratitude to my mother, father, and sister. Without them, I wouldn't be who I'm today, nor would I have been able to complete this work. I also extend to my thanks to Uğurcan Demirhan, who was always by my side and did everything he could to cheer me up during my toughest times.

I would like to thank to T B TAK for supporting my PhD studies through 119Z570, 124Z032 and 117Z213 projects and to Scientific Research Projects Coordination Office of METU for supporting my work via TEZ-D-118-2023-11114.

## TABLE OF CONTENTS

ABSTRACT.....	v
ÖZ .....	vii
ACKNOWLEDGMENTS .....	x
TABLE OF CONTENTS.....	xi
LIST OF TABLES .....	xiii
LIST OF FIGURES .....	xiv
CHAPTERS	
1 INTRODUCTION .....	1
1.1 Human Yippie Like (YPEL) Gene Family .....	1
1.2 <i>MOH1</i> as the yeast homolog of the human YPEL gene family .....	2
1.3 The Aim of the Study .....	5
2 MATERIALS AND METHODS.....	7
2.1 Homology modelling.....	7
2.2 Cell Strains and Growth Conditions.....	7
2.3 Western Blot.....	8
2.4 RNA isolation and RT-qPCR.....	9
2.5 Scanning Electron Microscopy .....	10
2.6 Fourier Transformed Infrared Spectroscopy (FT-IR) .....	11
2.7 RNA-Sequencing .....	13
2.7.1 RNA Isolation .....	13
2.7.2 RNA-Seq Analysis.....	13
2.7.3 Verification of RNA-Seq results with RT-qPCR.....	14
3 RESULTS .....	15

3.1	<i>In silico</i> analyses .....	15
3.2	Investigation of expression levels of <i>MOHI</i> and its protein product under stress conditions.....	17
3.3	Scanning Electron Microscopy .....	19
3.4	Fourier Transformed Infrared Spectroscopy (FT-IR).....	20
3.5	RNA-Sequencing .....	30
4	CONCLUSIONS AND FUTURE DIRECTIONS .....	35
	REFERENCES .....	41
	APPENDICES .....	61
A.	PRIMER LIST .....	61
B.	MIQE CHECKLIST .....	63
C.	Phyre2 RESULTS.....	67
D.	SEM IMAGES OF LOGARITHMIC AND STATIONARY PHASE CELLS .....	79
E.	DIFFERENTIALLY EXPRESSED GENE LIST .....	81
	CURRICULUM VITAE .....	83

## LIST OF TABLES

### TABLES

<b>Table 1.</b> Cell Strains used in this study .....	7
<b>Table 2.</b> IR band assignment of the spectral bands in the PCA loading plots and their explained variance for PC-1 and PC-2. ....	24
<b>Table 3.</b> Primers that are used in this study.....	61
<b>Table 4.</b> MIQE Checklist .....	63
<b>Table 5.</b> Moh1p Phyre2 Results (Confidence > 80).....	67
<b>Table 6.</b> YPEL2 Phyre2 Results (Confidence > 80) .....	73
<b>Table 7.</b> Differentially expressed genes when WT and moh1 $\Delta$ cells compared....	81

## LIST OF FIGURES

### FIGURES

<b>Figure 1.</b> Spot Test Results.....	4
<b>Figure 2.</b> In silico analyses of <i>moh1</i> and YPEL2 .....	16
<b>Figure 3.</b> Expression of <i>MOH1</i> and its protein product in the presence of H <sub>2</sub> O <sub>2</sub> ...	18
<b>Figure 4.</b> SEM Images of WT, <i>moh1</i> Δ , and <i>moh1-i</i> cells grown on solid media in the presence and absence of stress.....	20
<b>Figure 5.</b> PCA score plot, HCA dendrogram, and PCA loading plot of WT and <i>moh1</i> cells.....	23
<b>Figure 6.</b> The second derivative-vector normalized spectra of the WT and <i>moh1</i> Δ cells in the (A) 3050-2750 cm <sup>-1</sup> and (B) 1770-400 cm <sup>-1</sup> spectral regions.....	26
<b>Figure 7.</b> The quantitative changes in lipids in the WT and <i>moh1</i> Δ cells.....	27
<b>Figure 8.</b> The quantitative changes in membrane lipid order and fluidity in the WT and <i>moh1</i> Δ cells .....	28
<b>Figure 9.</b> The quantitative changes in protein in the WT and <i>moh1</i> Δ cells .....	29
<b>Figure 10.</b> The quantitative changes in beta-glucan and mannan in the WT and <i>moh1</i> Δ cells .....	30
<b>Figure 11.</b> Verification of RNA-Seq results via RT-qPCR.....	31
<b>Figure 12.</b> RNA Seq Results.....	32
<b>Figure 13.</b> SEM Images of WT, <i>moh1</i> Δ , and <i>moh1-i</i> cells at logarithmic phase in the presence and absence of stress.....	79
<b>Figure 14.</b> SEM Images of WT, <i>moh1</i> Δ , and <i>moh1-i</i> cells at stationary phase in the presence and absence of stress.....	80

## CHAPTER 1

### INTRODUCTION

17 $\beta$ -estradiol (E2), the primary estrogen hormone in the bloodstream, is crucial for the function of various organs and tissues. Effects of E2 on target cells are mediated by estrogen receptors (ERs)  $\alpha$  and  $\beta$ . When E2 binds to these receptors, they regulate the expression of genes that control cellular proliferation, differentiation, and death. Disrupted E2-ER signaling is a significant factor in the development of malignancies in target tissues. Given the critical role of E2-ER signaling in the health and disease of E2-responsive tissues, identifying estrogen-responsive genes and their protein products could aid in creating prognostic tools and therapeutic targets. In our research to better understand the genomic action of E2-ER, we previously identified Yippee Like 2 (YPEL2) as a gene responsive to E2-ER $\alpha$  signaling [1].

#### 1.1 Human Yippee Like (YPEL) Gene Family

*YPEL2* is a member of the human YPEL gene family, which is named after the Yippee gene found in *Drosophila*. This family includes 100 genes from 68 different species, spanning from yeast and plants to mammals, and exhibits a remarkably high degree of nucleotide sequence similarity [2]-[4]. The human YPEL family includes five YPEL genes, *YPEL1-5*, which arose from ancestral gene duplications and are located in different chromosomes. The expression of the YPEL family of genes is also mediated by common signaling pathways including growth factors and steroid hormones [5].

The YPEL family genes produce small proteins that share a high degree of amino acid sequence identity, which is predicted to form a zinc-finger-like metal binding pocket, known as the Yippee domain [2], [3]. This significant sequence similarity

among YPEL proteins leads to structural conservations that likely reflect functional commonalities. YPEL proteins are involved in similar cellular processes, including proliferation, senescence, and cell death [4], [6]-[22]. Consistent with these, deregulated YPEL gene expressions have been suggested to be associated with the initiation and/or development of various disorders, malignancies, and resistance to therapies [6], [12], [15], [20], [23]-[29].

Although YPEL proteins could be crucial in both physiological and pathological processes; the evolutionary conservation in nucleotide sequences, the ubiquity, and commonalities in the regulation of YPEL gene expressions, as well as structural similarities among YPEL proteins, render the deciphering of functional features of a YPEL protein in the presence of other YPELs in cellular processes difficult. To begin to address the function(s) of YPEL2, we recently attempted to identify the protein partners of YPEL2 utilizing an inducible heterologous expression system combined with dynamic proximity biotin labeling and subsequent mass spectrometry analyses in non-tumorigenic COS7 cells that endogenously synthesize YPEL proteins. Our findings revealed that YPEL2 interacts with proteins involved in various cellular processes, including responses to stress [30]. Based on these results, along with our observations that ectopically synthesized YPEL2 as endogenous YPEL proteins localize to stress granules in response to oxidative stress, we proposed that YPEL2 plays a role in cellular stress adaptation [30]. However, the mechanisms by which YPEL2 exerts its effects in cells remain unclear.

## **1.2 *MOH1* as the yeast homolog of the human YPEL gene family**

The basic mechanisms of cellular events including proliferation, metabolism, and death of the budding yeast *S. cerevisiae* share characteristics with evolutionarily distant species, including humans, due to its highly conserved gene homology [31]. This conservation enables the use of functional complementation approaches to study the characteristics of homologous proteins. The yeast genome contains a single YPEL gene ortholog: *MOH1*. Based on this, we predicted that complementing

*MOHI* in a yeast model with a YPEL gene could provide significant insights into the role of a YPEL protein in cellular processes, independent of other YPEL proteins. A limited number of studies suggest that the *MOH1* gene is essential for the stationary phase [32]. Cells with a deleted *MOH1* gene are unable to survive under nutrient-depleted stationary phase conditions [32], [33]. This is consistent with observations that the transition from the stationary phase to a nutrient-rich environment increases the expression of several genes, including *MOHI* [34]. Additionally, studies have shown that *MOHI*-deleted yeast cells (*moh1Δ*) show resistance to stress induction compared to wild-type (WT) strains when exposed to various stressors, such as UV irradiation, chemicals, heat, and hyperosmotic shock [22]. These studies collectively suggest that Moh1p, as the human YPEL2 protein, contributes to cellular stress responses. Studies also showed that the ectopic expression of *MOHI* or individual YPEL genes in the *moh1Δ* strain restores the WT phenotype in response to various stressors [22]. Moreover, during my Master studies, we established a yeast model in which we inserted the wild-type *MOHI* (*moh1-i*) and flag-tagged *MOHI* (*f-moh1-i*) cDNA into the genomic locus of *MOHI* in the *moh1Δ* yeast genome. Under normal growth conditions, we observed no difference between WT and *moh1Δ* in the manner of growth or survival (Figure 1C). We also confirmed the finding that the deletion of *MOHI* leads to a decrease in the colony-forming unit when the mutant strain was grown in water [33] as a nutrient-depleted stress environment [35] (Figure 1A).

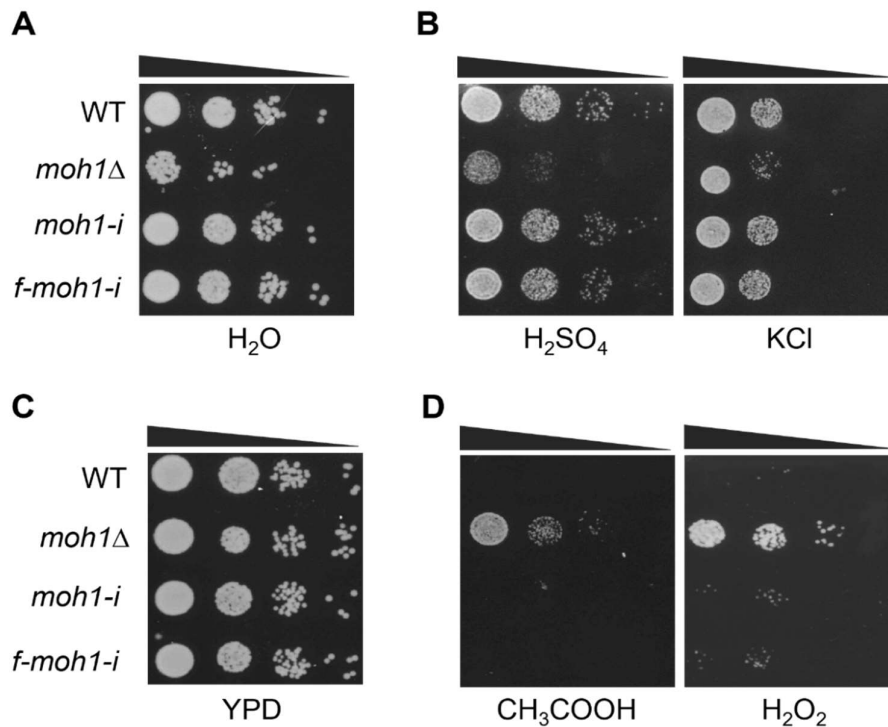


**Figure 1. Spot Test Results** **A)** Growth in water for 14 days **B)** Growth in the stress conditions H<sub>2</sub>SO<sub>4</sub> and KCl; in which the absence of *MOHI* leads to a decrease in survival rate. **C)** Growth on YPD Agar; Control Group **D)** Growth in the stress conditions CH<sub>3</sub>COOH and H<sub>2</sub>O<sub>2</sub>; in which the absence of *MOHI* provides a survival advantage.

Under oxidative stress induced by various concentrations of H<sub>2</sub>O<sub>2</sub>, the *moh1Δ* strain showed greater resistance and a higher survival rate compared to the WT strain (Figure 1D). Conversely, the *moh1Δ* strain had a lower survival rate than the WT strain when exposed to different concentrations of H<sub>2</sub>SO<sub>4</sub> as an acidic stress inducer (Fig 1B). When subjected to weak organic acid stress with acetic acid, the *moh1Δ* strain shows resistance similar to that observed with H<sub>2</sub>O<sub>2</sub> (Figure 1D). However, under hyperosmotic stress with KCl, the WT strain had a higher survival rate (Figure 1B). Thus, the absence of *MOHI* affects cell survival differently depending on the type of stress inducer. However, how the *moh1* protein (Moh1p) exerts its effect on cellular phenotype is unclear.

### 1.3 The Aim of the Study

Because the E2 signaling pathway plays a crucial role in cellular physiology and pathophysiology, identifying E2-responsive genes and their functions can be vital for the diagnosis and treatment of E2-mediated diseases. Therefore, we aimed to determine the function of *YPEL2*, an estrogen-responsive gene. *YPEL2* is a member of the *YPEL* family, which has high amino acid sequence homology. This structural similarity leads to functional commonalities, making it challenging to identify the function of *YPEL2* among other members of the *YPEL* family. Although we do not yet understand the mechanisms involved, we have found that *YPEL2* is associated with proteins involved in cellular stress responses and localizes to stress granules under oxidative stress conditions using inducible systems. To better understand the functions of *YPEL2*, we decided to use a yeast model, as yeast contains the only homolog of the *YPEL* family, *MOH1*. Our studies indicate that Moh1p plays a significant role in cellular stress responses and affects cellular survival differently under various stress conditions. However, we still do not know the specific mechanisms by which Moh1p contributes to cellular survival under stress conditions. These studies collectively suggest that Moh1p, as the human *YPEL2* protein, contributes to cellular stress responses.

Since the elucidation of functional features of moh1 could provide important clues about *YPEL* functions, in this study, we aimed to characterize the Moh1 protein by investigating how its presence and absence affect the cell's morphology, biomolecular/biochemical composition and transcriptomic profile. Through this study, we aimed to obtain better understanding to of Moh1p functions in the cell which leads to shed on the functions of *YPEL2* and other *YPEL* family members.



## CHAPTER 2

### MATERIALS AND METHODS

#### 2.1 Homology modelling

For the alignment of amino acid sequences, the Jalview application was used together with the Clustal W plug-in. The secondary structure analysis of moh1 and YPEL2 was carried out with the jPred4 online tool for the prediction of structural similarities. In addition to these, tertiary structure analysis was performed for moh1 and YPEL2 by using the Alphafold plug-in found in the ChimeraX molecular visualization program. The homology modeling studies for YPEL2 and Moh1p were carried out with the Phyre2 web tool.

#### 2.2 Cell Strains and Growth Conditions

All strains used in this study are derived from the *S. Cerevisiae* BY4741 strain (Table 1).

**Table 1.** Cell Strains used in this study

Name	Genotype	Abbr.
WT-BY4741	<i>MATa his3Δ1 leu2Δ0 met15Δ0 ura3Δ0</i>	WT
moh1Δ-BY4741	<i>MATa his3Δ1 leu2Δ0 met15Δ0 ura3Δ0 moh1Δ::KanMX4</i>	moh1
moh1Δ-By4741+WT-MOH1	<i>MATa his3Δ1 leu2Δ0 met15Δ0 ura3Δ0 moh1Δ::WT-moh1</i>	moh1-i
moh1Δ-By4741+flag-MOH1	<i>MATa his3Δ1 leu2Δ0 met15Δ0 ura3Δ0 moh1Δ::flag-moh1</i>	f-moh1-i

For the growth of the cell strains, yeast extract-peptone-dextrose medium (YPD) was used. This medium contains 1% yeast extract (Sigma, Germany, 70161), 2% dextrose (Sigma, Germany, 49159), and 2% peptone (Sigma, Germany, 912489). For the solid plates, 2% bacteriological agar was added to the culture. For the stress induction, “stress agar plates” were prepared. The autoclaved YPD-Agar medium was cooled down to 55°C and 3.25 mM H<sub>2</sub>O<sub>2</sub> was added onto this autoclaved YPD-Agar as stress inducer. For the selection of transformant cells URA(-) plates containing 0.67% yeast nitrogen base without amino acids (Sigma, Germany, Y0626), 2% dextrose, and 0.192% yeast synthetic drop-out medium supplement without uracil were used.

For the stress induction, short- and long-term stress were applied to cells. For the short-term stress, cells were grown in YPD at 30°C with reciprocal shaking at 180 rpm overnight. After this growth, cells were subcultured into a fresh YPD medium at 1:100 dilution and grown until the log phase (OD<sub>600</sub>=0.4-0.6). Then, H<sub>2</sub>O<sub>2</sub> with a final concentration of 3.25 mM was added into the culture and further incubated for 45 minutes at 30°C with reciprocal shaking. When incubation was terminated, cells were harvested and pelleted by centrifugation and processed for subsequent events. For the long-term stress induction, stress agar plates were used. Cells were grown as described in short-term stress induction. After cells were subcultured and they reached the log phase, cells were spotted on stress agar plates. These stress agar plates were incubated at 30°C for 40 hours. Cells were collected with a cell scraper into sterile water and pelleted for subsequent experiments.

### **2.3 Western Blot**

Cells were treated with short- or long-term stress as described in Section 2.2. Pelleted cells were washed with sterile distilled water and then re-suspended in 100 µl of urea-lysis buffer (40 mM Tris, pH=6.8; 0.1 mM EDTA; 5% SDS; 9M urea; 0.02 mg/ml bromophenol blue). 75 µl of glass beads were added onto resuspended cells. The mixture was vortexed 5 times for 1 minute with icing for 1 minute in between

vortexes. By using a hot syringe needle, the bottom of the tube was punctured and placed onto a new, clean tube and centrifuged at 4000 rpm for 2 minutes to separate glass beads. This mixture was then re-centrifuged for 15 min at 14000 rpm. After centrifugation supernatant was transferred into a clean tube.

After protein isolation, the same amount of protein (25  $\mu$ g) was loaded to 10% SDS-PAGE gel for western blot (WB) analysis. Proteins were run at 100 V for 1.5 hours. Proteins were then transferred by using a wet transfer system onto a PVDF membrane (Advansta, WesternBright™ PVDF-CL, L- 08008-001). The membrane was blocked with 5% skim milk in 0.1% Tris Buffered Saline-Tween (TBS-T). For the detection of proteins, a flag antibody (M2-Flag, Sigma-Aldrich, F-1804) was used in a 1:1000 dilution in TBS-T. After primary antibody incubation, the membrane was washed with 0.1% TBS-T 3 times for 5 min each. The membrane was then incubated with a goat anti-mouse-HRP antibody with a 1:4000 dilution (Santa Cruz Biotechnology, USA) for 1 hour and washed with TBS-T 3 times. For protein detection, the membrane was treated with WesternBright ECL substrate (Advansta, K-12045-D50) in a 1:1 luminol-enhancer reagent:peroxide reagent ratio in the dark for 2 min. Visualization was carried out with the ChemiDoc™ MP system (Bio-Rad, USA).

#### **2.4 RNA isolation and RT-qPCR**

Cells were subjected to short- or long-term stress as described in Section 2.2. Harvested cells were resuspended in 400  $\mu$ l of ice-cold acetate-EDTA (AE) buffer (50 mM sodium acetate; 10 mM EDTA, pH = 8) and then 25  $\mu$ l of 20% of SDS was added to the resuspended cells. The cell suspension was then mixed with 500  $\mu$ l of acidic phenol:chloroform:isoamyl alcohol (25:24:1; PCI) solution and incubated at 65°C for 15 minutes followed by incubation on ice for 10 minutes. After the first PCI incubation, samples were centrifuged for phase separation at 14000 rpm at 4°C for 15 minutes. The liquid phase was transferred into a clean microfuge tube and 500  $\mu$ l of acidic PCI solution was added into the liquid phase. This mixture was vortexed

for 20 seconds and incubated on ice for 10 minutes. Then samples were centrifuged again with the same conditions, the liquid phase was taken into a new microfuge tube and 1/10 volume of sodium acetate (pH = 5.3) and 3 volumes of 100% EtOH were added into the tubes. After incubation at -80°C for 30 minutes, the mixture was centrifuged to precipitate RNA at 14000 rpm at 4°C for 15 minutes. The precipitated RNA was air-dried for 15 minutes at most and then dissolved with diethylpyrocarbonate (DEPC)-treated water. RNA isolation was followed by DNase I treatment to remove genomic DNA from the sample. The DNA-free RNA samples were then converted into cDNAs with The RevertAid First Strand cDNA Synthesis Kit (Thermo-Fisher) with oligo (dT)<sub>18</sub> primers according to the manufacturer's instructions. For qPCR experiments, these cDNAs were used as templates, and experiments were carried out by using SsoAdvanced Universal SYBR Green SuperMix (Bio-Rad, USA) and transcript variant-specific primers (Table 3 in Appendices A). *FCY1* and *ALG9* were used as reference genes for normalization in the analyses, and the differential expression was shown as fold change using  $2^{-\Delta\Delta Ct}$  [36]. All of the RT-qPCR experiments were performed by following MIQE Guidelines (Table 4 in Appendices B) [37].

## 2.5 Scanning Electron Microscopy

For the scanning electron microscopy experiments, (1) WT, (2) *moh1Δ* and (3) *moh1-i* cells were grown until the logarithmic and the stationary phases, as well as on solid culture. For all these culture conditions, a single colony was selected into the YPD medium and grown overnight at 30°C with reciprocal shaking at 180 rpm. For cells grown until the logarithmic phase, cells were subcultured at a 1:100 ratio, and grown at 30°C with reciprocal shaking at 180 rpm until OD<sub>600</sub> reached 0.4-0.6. Then, half of the culture was subjected to short-term stress, and the other half was used as control. For cells grown until the stationary phase, we applied the same growth condition mentioned in the logarithmic phase except, after subculturing, cells were grown for 48 hours at 30°C with reciprocal shaking at 180 rpm. For the cells

on solid culture, after cells reached the logarithmic phase, they were counted with a hemocytometer, and 250 cells were seeded onto the YPD-Agar or stress agar plates. These plates were incubated for 40 hours at 30°C and then collected with a cell scraper. After growing cells from each phase, cells were washed with sterile water twice. Cells were pelleted at 1000 rpm for 5 minutes and mixed in 0.4% glutaraldehyde solution for fixation for scanning electron microscopy (SEM) visualization. SEM visualization was done by Prof. Dr. Zekiye Suludere and Prof. Dr. Demet Çetin at Gazi University.

## **2.6 Fourier Transformed Infrared Spectroscopy (FT-IR)**

The WT and moh1Δ yeast strains were grown overnight in the YPD medium at 30°C with reciprocal shaking at 180 rpm. After overnight growth, cells were subcultured into a fresh YPD medium with a 1:100 dilution. Cells grown to OD<sub>600</sub>=0.4 were then spotted on the YPD-Agar plates. Plates were incubated at 30°C for 40 hours. Cells were collected by a scraper from the agar plate into sterile distilled water and pelleted at 1000 rpm for 5 minutes by centrifugation. Cells were then washed with distilled water and 20x10<sup>7</sup> were resuspended in 5 μl of water. For FTIR studies, five biological replicates of WT and moh1Δ cells were used.

All FTIR readings were performed at the East Anatolia High Technology Application and Research Center of Atatürk University by using the Attenuated Total Reflectance (ATR) mode of FTIR spectroscopy (Bruker Vertex 70, Ettlingen, Germany). For this, 3 μl of concentrated yeast were placed on ATR crystal, and cells were dried with N<sub>2</sub> gas for 5 min. For each group, five spectra were collected with 2 technical replicas for each. Spectra were acquired with 32 scans in the 4000-400 cm<sup>-1</sup> spectral region at a spectral resolution of 4 cm<sup>-1</sup> by using the OPUS 7.5 (Bruker, Ettlingen, Germany) software. After each measurement, 70% ethanol and distilled water were used to clean the diamond crystal of the spectrometer.

Before chemometric analysis, spectral preprocessing was performed. For this, sample spectra were first smoothed (Savitzky-Golay smoothing, smoothing factor: 17) and the baseline was corrected using concave rubber band correction (iteration: 15; iteration number: 64). The Opus 5.5 software (Bruker, Germany) was then used to normalize the base-line corrected data as min-max in the 4000-400  $\text{cm}^{-1}$  spectral region.

For all unsupervised chemometric analysis, the Unscrambler® X 10.3 (CAMO Software AS, Norway) software was used. To determine the spectral differences between WT and moh1 $\Delta$  cells, principal component analysis was initially applied to the preprocessed spectra in the 4000-400  $\text{cm}^{-1}$  spectral region. For PCA, the mean-centered data, the full cross-validation method, and the singular value decomposition (SVD) algorithm were used. To provide support for the PCA score plot, hierarchical component analysis (HCA) was also performed by using Ward's algorithm and squared Euclidean distance measurements.

The average of sample spectra was first acquired and baseline-corrected to visually determine the spectral band differences between the WT and moh1 $\Delta$  groups. Then, their differences were calculated and given in the two main spectral regions of 3700–2750  $\text{cm}^{-1}$  and 1770–400  $\text{cm}^{-1}$ . To illustrate these variations between groups in detail, the second derivative of each group's average spectra data was obtained and vector-normalized. The main spectral bands were described on the PCA loading plot, and their contribution variance was calculated to elucidate the cellular macromolecular differences between the WT and moh1 $\Delta$  groups that contribute to their differentiation. The quantitative spectral analyses including the calculation of the band frequency, bandwidth, band area, and area ratio values were conducted in accord with previous studies [38], [39].

For testing the statistical significance of the quantitative spectral data, a student's t-test was performed via GraphPad Prism 6.0 statistics software (Graph Pad, La Jolla, CA). The data are presented as the mean  $\pm$  S.E.M, and  $P < 0.05$  was considered statistically significant.

## 2.7 RNA-Sequencing

### 2.7.1 RNA Isolation

For the RNA Sequencing experiments WT and moh1 $\Delta$  cells were used. Cells were grown on YPD-Agar plates and collected with a cell scraper into water. Harvested cells were used for RNA isolation as described in Section 2.4.

### 2.7.2 RNA-Seq Analysis

From each group, at least 2  $\mu$ g of RNA were used for sequencing. For RNA sequencing, RNA-seq libraries were performed with the BGISEQ-500 100bp double-ended sequencing approach [40] with a sequencing depth of at least 30 million. Results obtained after the sequencing process were subjected to quality control. Contaminants in the read data, adapter sequences, sequences below a certain base number (30 bases), and low-quality readings were filtered out. The clean readings obtained after the initial filtering were aligned to the most recent version of the *S. Cerevisiae* genome (Ensemble 101) using the STAR (Hierarchical Indexing for Spliced Alignment of Transcripts) software [41]. Transcript and gene count matrices were obtained with the featureCounts program after the alignment process [42]. The count data were used to analyze differentially expressed genes by using the DeSeq2 analysis [43]. For the multi-factor analysis, the WT group was used as the reference. After analysis, the threshold for adjusted p-value was 0.05 and the threshold for log fold change values at the base of logarithm 2 was determined as -1/+1. After the DeSeq2 analysis, differentially expressed genes (DEGs) are listed. All these analyses were conducted by using the R language [44]. We utilized the Metascape portal for GO analysis (<https://metascape.org/>) [45] with DEGs using a p-value of 0.05 as the threshold.

### **2.7.3 Verification of RNA-Seq results with RT-qPCR**

For the verification of RNA Sequencing results, the fractionally reserved RNA samples subjected to RNA-Seq were converted into cDNA libraries using the RevertAid First Strand cDNA Synthesis Kit (Thermo-Fisher) with oligo (dT)18 primers according to the manufacturer's instructions. For the verification of RNA-Seq results, three differentially expressed genes from RNA-Seq results were selected: *ALD3*, *GRE1*, and *SRL1* according to their functions in the cell. RT-qPCR experiments were carried out as described in Section 2.4 by using transcript-specific primer sets (Appendix A).

## CHAPTER 3

### RESULTS

#### 3.1 *In silico* analyses

Protein functions are largely derived from their structural characteristics. Amino acid homologies between two proteins within a protein family can be used to predict structural similarities [46]. Based on this, we initially examined the structural similarities between the human YPEL proteins and the yeast homolog Moh1p. We started the *in silico* analysis with primary sequence homology alignment for Moh1p and YPEL2. For this analysis, we used the Jalview software [47] (<https://www.jalview.org/>) with the ClustalOmega plug-in [48]. Our results for the human YPEL gene family were consistent with the previous studies [2], [3] in which YPEL 1-4 were shown to share between 83.2-96.6% amino acid sequence homology, while YPEL5 shows the lowest sequence identity to other YPEL proteins ranging from 43.8 to 49.5%. In addition, Moh1p shows 37.8% amino acid sequence homology with YPEL2 while the amino acid identity ranges from 31.4%-40.2% with other YPEL proteins (Figure 3A). For the secondary structure homology analysis of Moh1p and YPEL2, we used the JPred4 server (<http://www.compbio.dundee.ac.uk/jpred4/index.html>) [49]. This analysis indicated that both of the proteins mostly comprised beta sheets (Figure 3B). Along with these, by using the AlphaFold server (<https://alphafold.ebi.ac.uk/>) [50], [51] with the ChimeraX molecular visualization software (<https://www.cgl.ucsf.edu/chimerax/>), [52], [53], we carried out the tertiary structure prediction analysis. According to the results, both Moh1p and YPEL2 fold into globular structures except for the immediate amino-terminus regions, which are distinct (Figure 3C). Lastly, we used the Phyre2 server [54], (<http://www.sbg.bio.ic.ac.uk/~phyre2/html/page.cgi?id=index>) to analyze the

structural homologs of moh1 and YPEL2. The Phyre2 results indicated that Moh1p and YPEL2 matched with multiple protein families (PDB headers), including ligase, RNA binding, hydrolase, oxidoreductase, and Mss4-like, with probabilities of more than 90% confidence (Figure 3D, Table 5 and 6 in Appendices C).

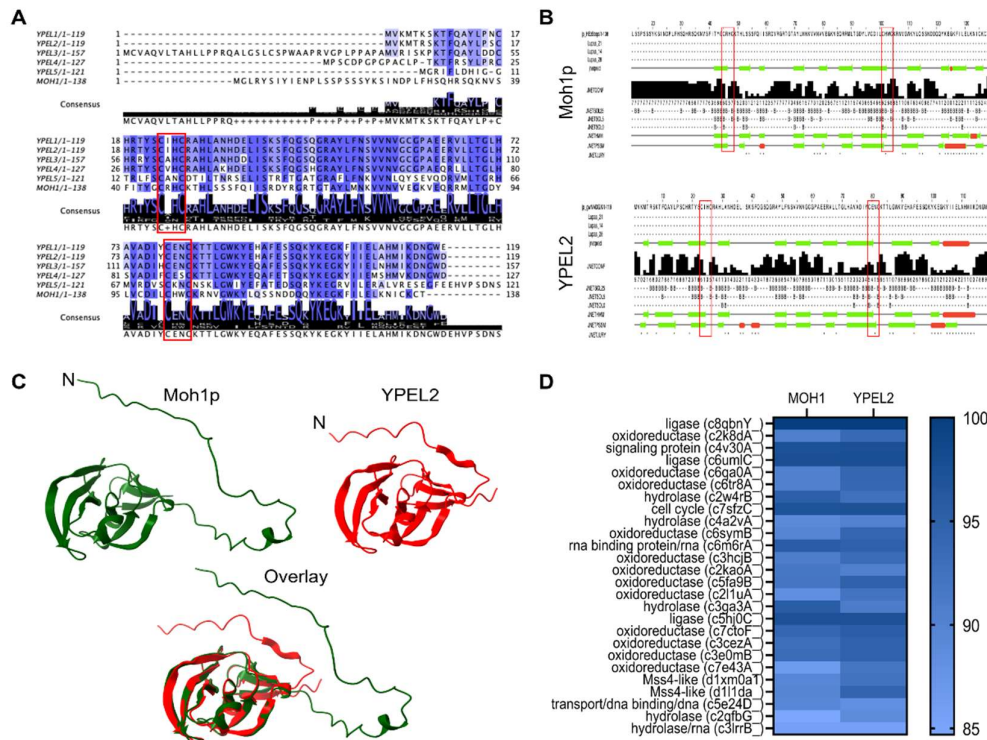


**Figure 2. In silico analyses of moh1 and YPEL2. A.** The alignment of the amino acid sequence of YPEL proteins and moh1 **B.** Secondary structure analysis of Moh1p and YPEL2 via the jPred server **C.** Prediction and superimposition of tertiary structures of YPEL2 and Moh1p **D.** Homology modeling of YPEL2 and Moh1p with the Phyre2 server.

Our recent studies showed that YPEL2 may be involved in stress surveillance in model cells [30]. In addition, we showed that Moh1p exhibits different effects on the survival rate of yeast cells under different stress conditions (Figure 1). The structural similarities of Moh1p and YPEL2, the homology of Moh1p and YPEL2 to protein families of oxidoreductases, and the possible function of YPEL2 in stress surveillance mechanisms suggest that Moh1p and YPEL2 might have evolutionarily conserved common functions in cells.

### **3.2 Investigation of expression levels of *MOHI* and its protein product under stress conditions**

Observations that the *moh1Δ* cells cannot survive under nutrient-depleted stationary phase conditions [32], [33] suggest that *MOHI* is a stationary phase-essential gene [32]. This is also consistent with the findings that the exit from the stationary phase in response to a nutrient-rich environment augments the expression of a set of genes including *MOHI* [34]. Moreover, the *moh1Δ* strain exhibits enhanced cell viability in response to various stressors including UV irradiation, chemicals, heat, and hyperosmotic shock compared with the WT strain [22]. Furthermore, the ectopic expression of *MOHI*, as individual YPEL genes, in the *moh1Δ* strain was reported to restore WT phenotype in response to various stressors [22], as I also showed during my Master studies that the *moh1Δ* strain compared to WT cells exhibits resistance to H<sub>2</sub>O<sub>2</sub> as an oxidative stress inducer. These results are consistent with the prediction that Moh1p contributes to cellular stress responses.

Since very little is known about the functional features of Moh1p, before embarking on studies aimed at the dissection of YPEL2 functions on cellular processes through functional complementation in yeast, I wanted to explore the molecular events affected by the *MOHI* gene. Based on our *in silico* analysis Moh1p may belong to the oxidoreductase family, I continued to use H<sub>2</sub>O<sub>2</sub> as the stress inducer for my studies on Moh1p functions.

To understand whether *MOHI* expression levels are altered under stress conditions, I subjected WT, *moh1Δ*, and *f-moh1-i* cells to short- and long-term H<sub>2</sub>O<sub>2</sub> stress. After stress induction, RNAs isolated from cells were converted into cDNA. By using these cDNAs as the template, RT-qPCR was performed. According to RT-qPCR results, either the short- or long-term H<sub>2</sub>O<sub>2</sub> exposure leads to the repression of the expression of *MOHI* in WT or *f-moh1-i* cells. As expected, we could not detect the presence of transcripts from the samples isolated from *moh1Δ* (Figure 3A and B).

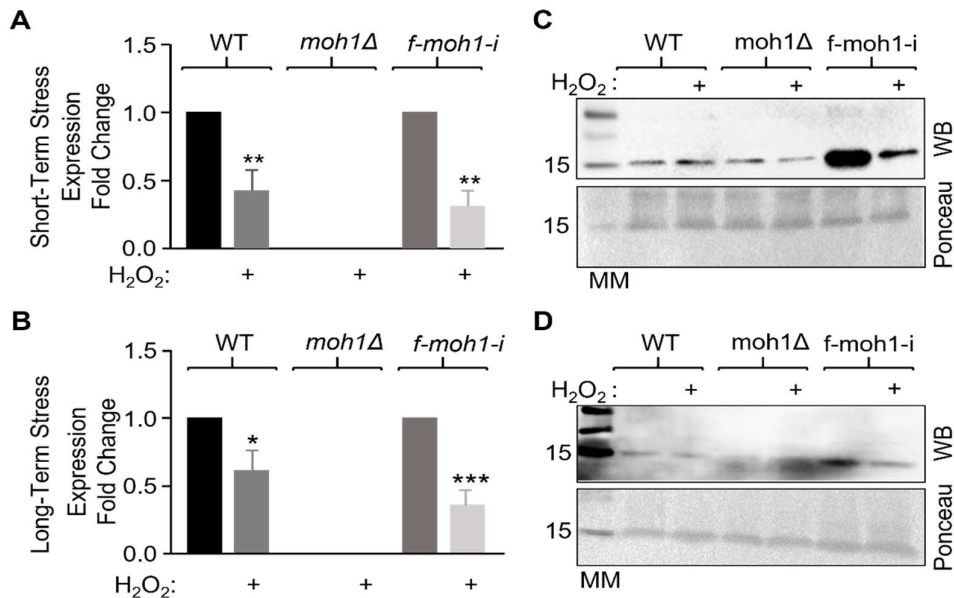


**Figure 3. Expression of *MOH1* and its protein product in the presence of H<sub>2</sub>O<sub>2</sub>.** Expression levels of *MOH1* in WT, *moh1Δ*, and *f-moh1-i* cells **A**. After exposure to short-term stress **B**. After exposure to long-term stress. Expression of *MOH1* was normalized to *ALG9* as the internal control. Protein levels of f-Moh1p in WT, *moh1Δ*, and *f-moh1-i* cells **C**. After exposure to short-term stress **D**. After exposure to long-term stress. For WB analysis, Ponceau staining was used as a control for equal loading.

We also examined the levels of Moh1p by using Western Blot (WB). Due to the absence of an antibody specific to Moh1, I used the Flag antibody for the detection of f-Moh1p in the *f-moh1-i* strain. It was unexpected to detect any protein with the Flag antibody in samples from WT and *moh1Δ*. Unfortunately, however, the Flag antibody recognizes a non-specific protein species that shows molecular mass similar to the *f-moh1* protein. Nevertheless, our results clearly showed that both short- and long-term H<sub>2</sub>O<sub>2</sub> exposure leads to a decrease in the levels of the *f-moh1* protein (Figure 3C and D). This indicates a positive correlation between the expression of *MOH1* and Moh1 protein levels which decrease in response to H<sub>2</sub>O<sub>2</sub> stress.

### 3.3 Scanning Electron Microscopy

While examining yeast cells under the microscope, we noticed that although the number of cells remains similar among strains, the *moh1* $\Delta$  cells compared to WT are of smaller sizes and tend to clump (data not shown). Since clumping can occur when the separation of cells or septum formation is affected [55], [56], we decided to examine whether strains exhibit distinct structural/morphologic features that could account for our microscopic observations. For this, we decided to use scanning electron microscopy (SEM), which is frequently utilized to study the ultrastructure of biological sample surfaces to provide important information about cellular morphology and topography [57], [58]. We subjected WT, *moh1* $\Delta$ , and *moh-i* cells grown in different growth conditions (logarithmic, stationary, and growth on solid media) without or with H<sub>2</sub>O<sub>2</sub> as the oxidative stress inducer to SEM.

SEM images revealed differences in cell morphology. While the WT and *moh1* $\Delta$ -i strains showed similar cell sizes and ovoid morphology with smooth surfaces under all growth conditions, the *moh1* $\Delta$  strain cells displayed a pronounced spherical shape with a rough surface topology manifested as protrusions/indentations (Fig 4A and C, Figure 12 in Appendices D). Quantitative analyses further revealed that indeed the shape and the size of the *moh1* $\Delta$  cells differ from the WT or *moh1* $\Delta$ -i strain cells as assessed with analyses of a minimum of 50 cells from each strain by using ImageJ software [59] independently of H<sub>2</sub>O<sub>2</sub> stress (Fig 4B and D). These results suggest that the deletion of *MOHI* leads to alterations in cell morphology.

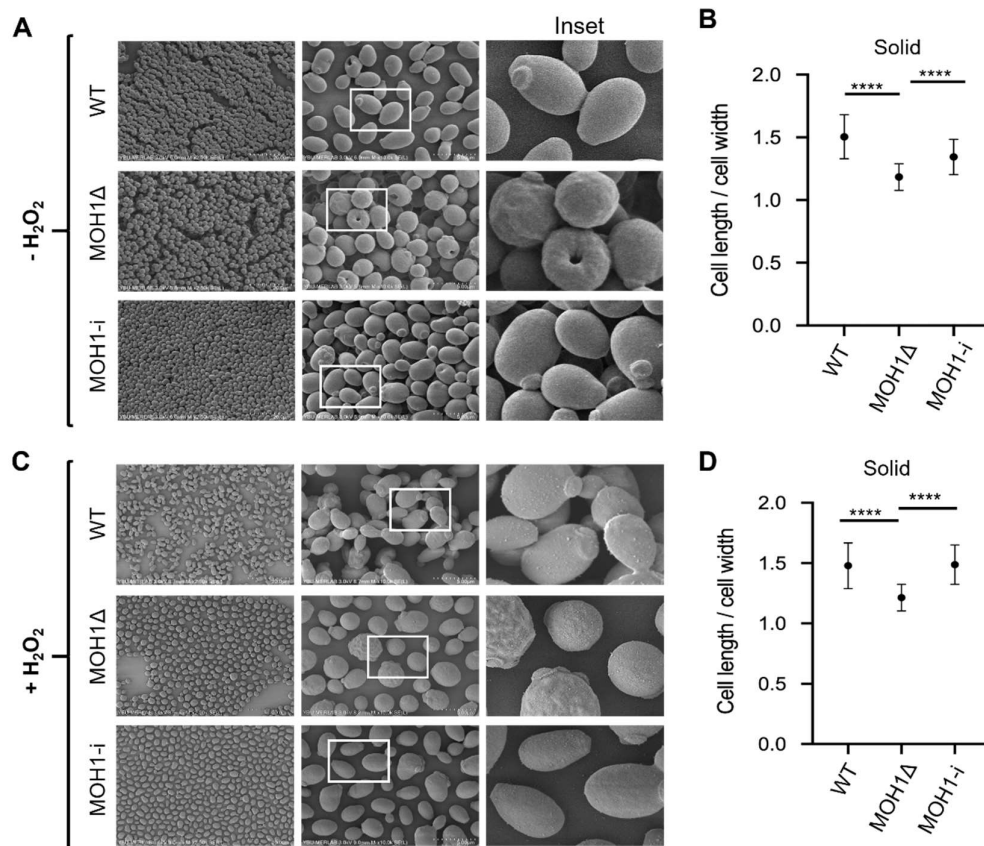


**Figure 4. SEM Images of WT, moh1Δ, and moh1-i cells grown on solid media in the presence and absence of stress.** **A.** SEM images in the absence of H<sub>2</sub>O<sub>2</sub>. White squares indicate Inset images. **B.** Cell length and width ratio in the absence of H<sub>2</sub>O<sub>2</sub>. **C.** SEM images in the presence of H<sub>2</sub>O<sub>2</sub>. White squares indicate Inset images. **D.** Cell length and width ratio in the presence of H<sub>2</sub>O<sub>2</sub>. Student t-test was conducted among groups for statistical difference. \*\*\*\* indicates significant difference ( $p < 0.001$ ).

### 3.4 Fourier Transformed Infrared Spectroscopy (FT-IR)

SEM analysis revealed that there is a morphological difference between moh1Δ cells and WT cells regardless of the stress exposure. This difference, which appears to occur specifically in the cell membrane and/or cell wall, could arise from the differences in the composition and arrangement of cellular macromolecule components.

The yeast cell wall is a dynamic structure that undergoes continuous remodeling during cell growth, division, and in response to environmental changes to maintain the shape and structural integrity of the cell crucial for cellular function and survival [60], [61]. There are three main components of the yeast cell wall: beta-glucans, mannoproteins, and chitin. Approximately 50-60% of the cell wall mass consists of beta-glucans and 40-50% mannoproteins. The main beta-glucans found in cell wall are  $\beta$ -(1,3)-glucan and  $\beta$ -(1,6)-glucan.  $\beta$ -(1,3)-glucan is the amorphous component of the cell wall and has a microfibrillar coiled spring-like structure that provides the cell wall with elasticity and tensile strength.  $\beta$ -(1,6)-glucan on the other hand forms a highly branched structure that crosslinks  $\beta$ -(1,3)-glucans and other cell wall components including mannoproteins and chitin [62]-[64]. Mannoproteins are non-filamentous glycoproteins linked with a glycosyl-phosphatidylinositol (GPI) anchor to the plasma membrane and are localized to the outermost layer of the yeast cell wall. Mannoproteins are connected by  $\beta$ -1,6-glucan chains to the innermost, fibrous layer formed of  $\beta$ -1,3-glucan chains and chitin [62], [63]. Chitin is a linear polymer glycosidically linked to non-reducing ends of  $\beta$ -(1,3)-glucan and  $\beta$ -(1,6)-glucan branches. Chitin is a long-chain polymer of N-acetylglucosamine represents little in mass (approximately 1-3%) compared to beta-glucans and mannoproteins in the yeast cell wall. By interconnecting cell wall components, chitin is critical for strengthening and maintaining the structural integrity of the cell wall as well as spetum and bud scars [62], [63].

The highly dynamic plasma membrane of yeast cells contains similar amounts of proteins and lipids and acts as a barrier between the cytoplasm and cell wall [65]. Proteins on the membrane are responsible for regulating the entry and exit of substances, including enzymes catalyzing the cell wall formation or receptors, into the cell [66]. The lipid composition of the membrane is highly diverse containing mainly phospholipids (glycerophospholipids, PL), sphingolipids, and sterols, and affects the activity of proteins in the cell membrane [66], [67]. Phospholipids of the cell membrane have an amphipathic character due to their hydrophobic diacylglycerol content and hydrophilic polar head groups. While the physical

properties of PLs are determined by different polar groups, the diverse nature of PLs is provided by the unsaturated and saturated fatty acid composition of diacylglycerol moiety [67]. In the cell, most of the sphingolipids are found in the membrane (approximately 90%). Sphingolipids have a sphingoid backbone and are produced only by the cell wall-generating eukaryotes critical for cell growth. Inositol phosphate is attached to the ceramide which is formed by binding to a saturated fatty acid to the long-chain sphingoid backbone. Sphingolipids are crucial for the proper growth of cells [66]-[68]. Sterols are the nonpolar lipid class in the yeast plasma membrane. The main sterol form in *S. Cerevisiae* is ergosterol (Erg) which is the human equivalent form of cholesterol. Although sterol synthesis is vital for cell and cell membrane integrity, sterol synthesis is tightly regulated since the accumulation of free sterols leads to toxicity in cells [67]. The close arrangement of sphingolipids and sterols is crucial for correct sorting proteins from the Golgi apparatus to the plasma membrane and plasma membrane functions [69].

Our observations with SEM revealed morphological differences between the WT and *moh1Δ* cells independently of H<sub>2</sub>O<sub>2</sub> as an oxidative stress inducer (Figure 4). These observations raise the possibility that the deletion of *MOHI* leads to alterations in the biomolecular composition of cells. To examine this issue, we conducted Fourier Transform Infrared Spectroscopy, FTIR, analyses. FTIR spectroscopy allows the elucidation of the chemical properties of biomolecules including proteins, lipids, nucleic acids, or polysaccharides of a biological sample, and generates sample-specific distinct molecular fingerprints [70]-[78]. Previous studies using FTIR spectroscopy investigated biomolecular changes in yeast exposed to many different conditions including stress responses, toxicity, and apoptosis [79]-[87]. A single infrared spectrum, IR, of a cell sample contains a large of spectral data points, as many as thousands, requiring various chemometric or advanced statistical methods for analysis [88]-[97]. One of the chemometric methods used with FTIR is principal component analysis (PCA). By converting data into a collection of orthogonal components, PCA decreases the dimensionality of large datasets and simplifies the complexity of the data. Variables called as principal components (PC)

effectively capture the most important variations in the data, facilitating the visualization and interpretation of patterns [98]-[101]. For the description of the correlation between *moh1Δ* and WT cells, we performed PCA on preprocessed spectra of these groups. The PCA score graph for WT and *moh1Δ* cells was plotted by PC1 and PC2 (Figure 5A), in which PC1 denotes the highest spectral variation while PC2 indicates the second highest spectral variation. Results show a 98% variance between the WT and *moh1Δ* cell groups (PC1:96%+PC2:2%) and demonstrate a considerable difference in their biomolecular contents. In addition to the PCA score plot, we also performed hierarchical clustering analysis (HCA) on the spectra of the WT and *moh1Δ* cells. HCA is a highly efficient method for categorizing and distinguishing distinct samples. This method organizes similar spectral data into clusters and thus, determines the distance between the biological samples [102], [103].

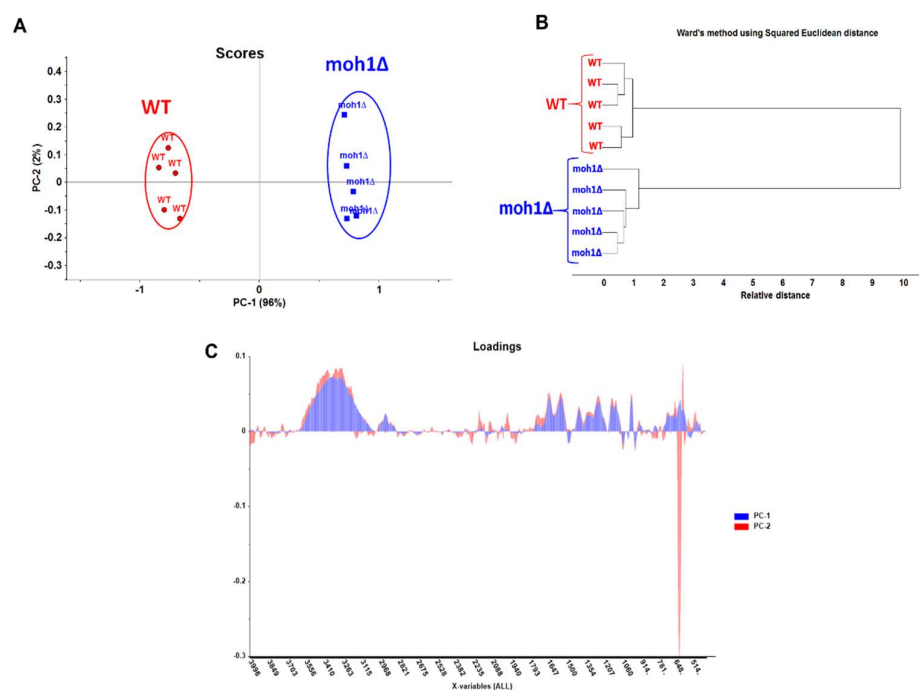


**Figure 5. PCA score plot, HCA dendrogram, and PCA loading plot of WT and *moh1* cells. A. PCA score plot B. HCA dendrogram C. PCA loading plots for the PC-1 and PC-2.**

HCA analysis, depicted as an HCA dendrogram in Figure 5B, reveals distinct clustering of WT and moh1Δ cells with a high relative distance value. The HCA result is also consistent with the PCA score finding. We also examined the PCA loading plots and spectra to quantitatively clarify the main spectral features, contributing to their accurate segregation. PCA loading plots highlight the critical wavenumbers that most significantly affect data variation. Thus, these plots enable the differentiation of various sample types or conditions [104]. The y-axis of the PCA loading plot denotes the eigenvalue. The high eigenvalue of a spectral band indicates that this peak has a great impact on the discrimination between the groups. Hence, we determined the wavenumber of these peaks and calculated their variances from the PC1 and PC2 loading spectra, shown in Figure 5C, together with band variance values and their assignments depicted in Table 2. For these bands, we obtained high variance values exceeding 70% indicating that the protein, lipid, triglyceride, nucleic acid, mannan, and beta-glucan contents of the WT and moh1Δ cell groups differ.

**Table 2.** IR band assignment of the spectral bands in the PCA loading plots and their explained variance for PC-1 and PC-2.

WT vs moh1Δ				
Band Location	PC1	PC2	Band Assignment	Reference
3289	99.80	99.87	Amide A: proteins	[105]
3064	95.75	96.18	Amide B: proteins	[105]
3005-3010	5.14	11.75	Olefinic group =CH: unsaturated lipids	[106]
2964	91.68	91.76	$\nu_{\text{asym}} \text{CH}_3$ lipids	[107]
2925	98.43	98.44	$\nu_{\text{as}} \text{CH}_2$ (lipids)	[107]
2855	85.23	85.92	$\nu_{\text{s}} \text{CH}_2$ (lipids)	[107]
1745	94.91	97.69	$\nu \text{C} = \text{O}$ ester of lipids	[108]
1638	99.74	99.79	Amide I: proteins, C = O stretching: $\beta$ sheet structure	[109]
1532	99.22	99.33	Amide II: proteins, $\delta \text{N-H}$ (bending) and $\nu \text{C-N}$ (stretching)	[107]

**Table 2.** (Continued)

<b>WT vs moh1Δ</b>				
<b>Band Location</b>	<b>PC1</b>	<b>PC2</b>	<b>Band Assignment</b>	<b>Reference</b>
<b>1454</b>	65.75	65.78	Various CH <sub>2</sub> /CH <sub>3</sub> bending vibrations in lipids and proteins	[107]
<b>1395</b>	99.47	99.51	Carboxylates of amino acids and δSCH <sub>2</sub> of lipids	[80]
<b>1344</b>	99.43	99.49	CH <sub>2</sub> wagging vibrations in lipids	[110]
<b>1307</b>	99.32	99.40	Amide III: C–N and C–O stretching, N–H and O C–N bending: protein	[107]
<b>1236</b>	99.65	99.48	v <sub>asym</sub> PO <sub>2</sub> <sup>−</sup> in DNA, RNA, and phospholipids	[107]
<b>1135</b>	99.66	99.78	Mannans and β1,3 glucans	[111]
<b>1064</b>	94.31	95.20	v <sub>sym</sub> C–O–C of nucleic acids and phospholipids	[112]
<b>1030</b>	75.21	75.57	β1,4 glucan	[111]
<b>993</b>	98.42	98.48	β1,6 glucan	[111]
<b>970</b>	94.42	95.15	Mannans	[111]
<b>916</b>	79.87	80.24	Pyranose ring asymmetric vibrations	[113]
<b>810</b>	92.79	95.78	Mannans	[111]

To visually present the spectral differences between the WT and moh1Δ cell groups, spectral preprocessing procedures, including second derivative and vector normalization analysis, were applied to the average sample spectra of each group. Results indicate (Figure 6) distinct spectral regions. The first region corresponds to unsaturated and saturated lipid-associated spectral bands, located between 3050 and 2750 cm<sup>−1</sup> (Figure 6A). On the other hand, the second spectral region is called as fingerprint region, located between 1770 and 400 cm<sup>−1</sup> (Figure 6B) and includes specific biomolecular-associated spectral peaks unique for yeast strain. These peaks are attributable to triglycerides, proteins, nucleic acids, mannans, and beta-glucan. According to these results, there are notable differences in the intensity and wavenumber of the spectral bands of the WT and moh1Δ groups.

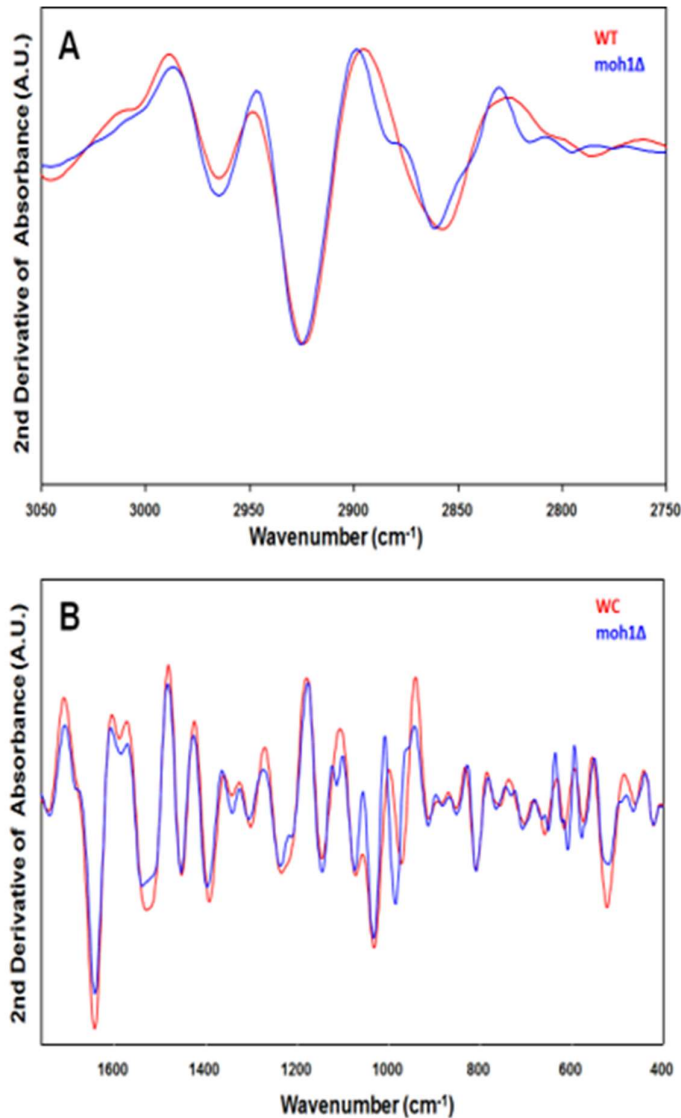


**Figure 6. The second derivative-vector normalized spectra of the WT and moh1Δ cells in the (A) 3050-2750 cm<sup>-1</sup> and (B) 1770-400 cm<sup>-1</sup> spectral regions.**

To elucidate the quantitative information of cell components from the FTIR spectral data, peak shifts, bandwidths, band area, and area ratios can be used. To compare the FTIR spectra of the WT and moh1Δ cells quantitatively, we calculated the band area ratio, the shift in the wavenumber, and the bandwidths of the spectral bands.

We initially analyzed variations of lipid-associated spectral bands of these two groups (Figure 7). Lipids play crucial roles in maintaining cell membrane integrity,

signaling, and energy storage, and their composition can significantly impact the ability of cells to withstand and adapt to various stress conditions including oxidative stress. To determine the unsaturated lipid content, we used the area ratio of unsaturated and saturated lipid content ( $A_{3005}/A_{2855+2925}$ ) of the WT and *moh1* $\Delta$  cells. Results revealed that there is a significant decrease in the content of unsaturated fatty acids in *moh1* $\Delta$  cells compared to the WT strain (Figure 7A). In addition to the unsaturated lipid, we examined the amount of saturated lipids and acyl chain length by taking the band area ratios of the related bands,  $A_{2855}/A_{2855+2925}$  and  $A_{2925}/A_{2964}$ , respectively (Figure 7B and C). Results indicate that the unsaturated and saturated lipid concentrations as well as acyl chain length in *moh1* $\Delta$  cells compared to the WT strain decreased significantly. Furthermore, the  $A_{1745}/A_{2855+2925}$  ratio of the triglyceride-cholesterol ester concentration of *moh1* $\Delta$  cells increased dramatically compared to that of the WT strain (Figure 7D).

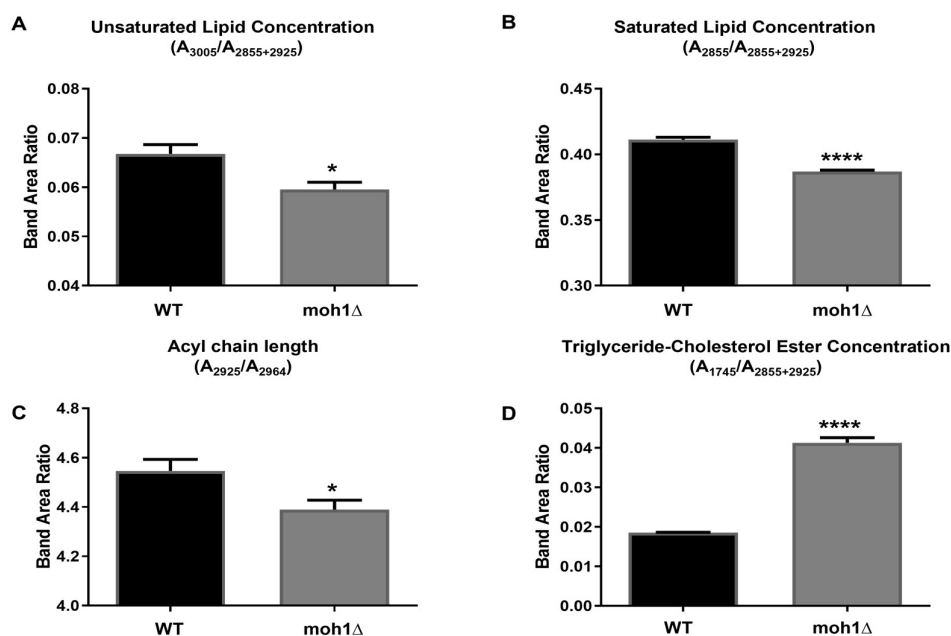


**Figure 7. The quantitative changes in lipids in the WT and *moh1* $\Delta$  cells. A)** unsaturated lipid, **B)** saturated lipid, **C)** triglyceride-cholesterol ester, **D)** acyl chain length of fatty acids (\* $p < 0.05$ , \*\*  $p < 0.01$ , \*\*\*\* $p < 0.0001$ ).

Since the lipid compositions show differences between the WT and *moh1* $\Delta$  cells, we also examined the lipid order or the degree of lipid packing. FTIR results showed

that membrane lipid order as an indication of tightly packed lipid molecules within membranes increases in *moh1Δ* cells compared to the WT cells (Figure 8A). Collectively these results suggest that the membrane fluidity of *moh1Δ* cells is decreased (Figure 8B). Referring to the viscosity of the lipid bilayer of a cell membrane, membrane fluidity is essential for maintaining the functionality and integrity of the cell membrane, ensuring that cellular processes occur efficiently in response to varying internal and environmental conditions [114], [115]. The symmetric and asymmetric stretching vibrations of the methylene (CH<sub>2</sub>) groups in the fatty acid chains of lipids are sensitive to the packing and order of the lipid molecules and can be effectively assessed with FTIR spectroscopy. The lower frequency of the CH<sub>2</sub> stretching mode (2964-2855 cm<sup>-1</sup> spectral regions) suggests a decrease in membrane fluidity, as the lipid chains are more ordered and more tightly packed [114], [116]. Indeed, we observe that the *moh1Δ* cells exhibit a substantially reduced membrane fluidity compared to the WT cells.

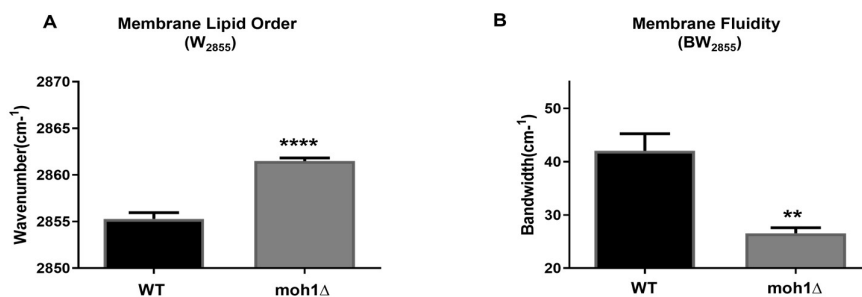


**Figure 8. The quantitative changes in membrane lipid order and fluidity in the WT and *moh1Δ* cells. A. Membrane lipid order B. Membrane fluidity (\*p < 0.05, \*\* p < 0.01, \*\*\*\*p < 0.0001).**

Consistent with changes in lipids, membrane proteins significantly contribute to the regulation of membrane fluidity through lateral mobility, density, conformational changes as well as interactions with lipids. To assess whether the *MOHI* deletion affected cellular proteins, we calculated the protein concentration as the band area ratio of amide II/amide I + amide II (48). Results suggest a decline in protein concentration in the *moh1Δ* strain compared to the WT cells (Figure 9A). On the

other hand, conformational changes in proteins as the band area ratio of the amide I/amide II ( $A_{1638}/A_{1524}$ ) increased significantly in *moh1* $\Delta$  cells compared to WT cells.

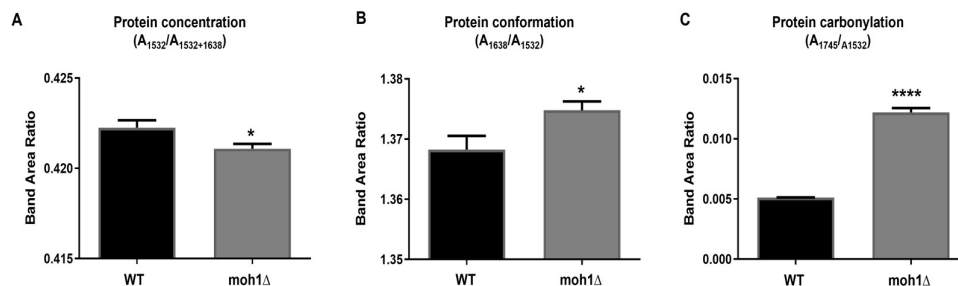


**Figure 9. The quantitative changes in protein in the WT and *moh1* $\Delta$  cells** A) protein concentration B) protein conformation and C) protein carbonylation (\* $p < 0.05$ , \*\*\*\* $p < 0.0001$ ).

Protein carbonylation is a common form of protein oxidation where carbonyl groups ( $-C=O$ ) are introduced into proteins, often as a result of oxidative damage which is associated with various pathological conditions and aging [117]. In addition to changes in protein concentrations and conformations, FTIR results also suggest carbonylation of proteins as the band area ratio  $A_{1745}/A_{1532}$  (49) increases dramatically in *moh1* $\Delta$  cells compared to WT cells.

The interplay between proteins and lipids is crucial for maintaining the dynamic nature of biological membranes, essential for various cellular functions and responses to environmental changes. Since the WT and *moh1* $\Delta$  cells show distinct cellular morphology assessed with SEM, we also wanted to examine the components of the cell wall. . For this, we computed the band area ratio of beta-glucan- and mannan-associated spectral bands (Figure 10). There is a substantial increase in the  $\beta$ -(1,6)- and  $\beta$ -(1,3)-glucan contents as well as mannan concentration of *moh1* $\Delta$  cells compared to WT cells (Figure 10). An increase in  $\beta$ -(1,6)-glucan,  $\beta$ -(1,3)-glucan, and mannan concentrations suggests reinforcement of the cell wall of *moh1* $\Delta$  cells.

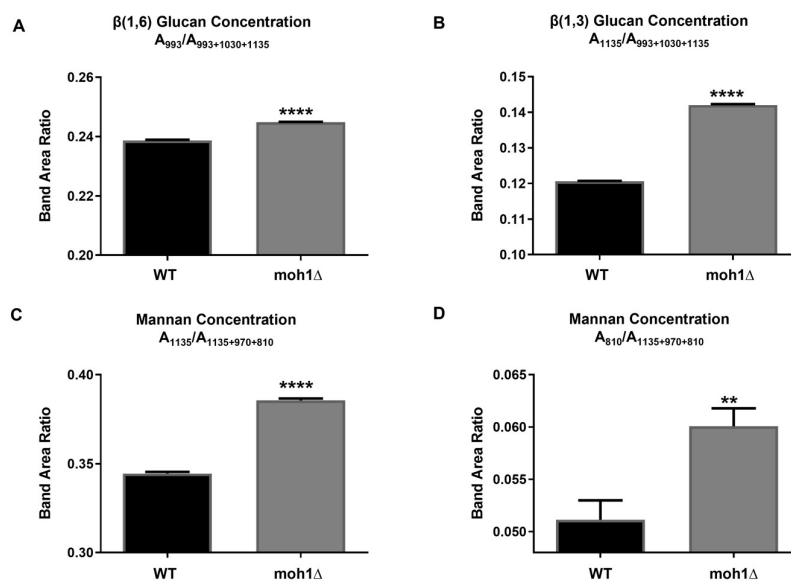


**Figure 10. The quantitative changes in beta-glucan and mannan in the WT and moh1Δ cells. A) β-(1-6)-Glucan, B) β-(1-3)-Glucan C) Mannan concentrations D)Mannan concentrations (\*\*:  $p < 0.01$ ,\*\*\*\*:  $p < 0.0001$ ).**

Thus, the deletion of *MOHI* appears to lead to a sequence of events dramatically altering biomolecule compositions, structures, and interactions. These alterations in turn could result in changes in membrane permeability and cell wall rigidity that are manifested as morphological differences between the WT and moh1Δ cells as we observe with SEM.

### 3.5 RNA-Sequencing

To assess the underlying molecular events leading to differences in biomolecular and morphological changes as a result of the *MOHI* deletion, we initially examined the transcriptomic profiles of the WT and the moh1Δ strains. For this, total RNA from cells was subjected to high-throughput RNA sequencing (RNA-Seq). We analyzed RNA-Seq results by using the DeSeq2 package in R. The threshold of log2 fold change was determined as -1/+1, and the threshold of adjusted p-value was determined as 0.05 for the identification of differentially expressed genes (DEGs). Results indicated that 43 genes, including *MOHI* as expected, are differentially

(Table 7 in Appendices E), expressed in the *moh1* $\Delta$  strain compared to the WT cells. We also verified the differential expression of *ALD3*, *GRE1*, and *SRL1* (Figure 11) which we selected as contributing components for stress responses and cell wall integrity [118]-[121].

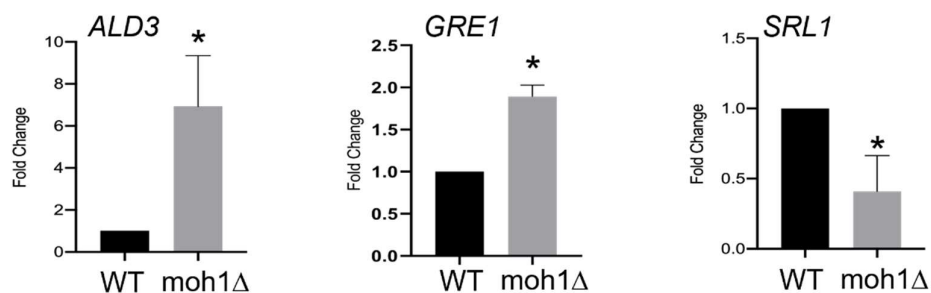


**Figure 11. Verification of RNA-Seq results via RT-qPCR.** Expression of genes was normalized to *ALG9* and *FCY1* as the internal control. \* indicates the significant change in the expression.

To assess gene ontologies of DEGs affected by the *MOH1* deletion for biological functions, we analyzed RNA-Seq results with the Metascape portal (<https://metascape.org/>), which is an integrated web-based system that allows functional enrichment, interactome analysis, gene annotation, and membership search [45].

We also used the STRING database (<https://string-db.org/>), which is an integrated publicly available source of protein-protein interaction information for performing gene-set enrichment analysis and visualization of interaction networks using various classification systems including Gene Ontology and KEGG [122]. Both database analyses revealed that 12 DEGs encode dubious open reading frames or are putative proteins with unknown functions. These DEGs are *YCR018C-A*, *YDL218W*, *YDR048C*, *YGL177W*, *YHR214W-A*, *YJR115W*, *YKL068W-A*, *YMR324C*, *YNL234W*, *RRT1*, *PAU19* and *YLL067C*. The analysis of the remaining DEGs revealed enrichments in the GO-terms of metabolic pathways (KEGG: *sce01100*) and glycolysis (R-SCE-70171). As components of metabolic pathways (KEGG: *sce01100*), differentially expressed genes include *PMT2*, *SUR2*, *YBR242W*, *PDC6*, *THI4*, *CYS4*, *SOR1*, *PFK27*, *ALD3*, *SNO4*, *ERR3*, *ERR2* and *MET6*. Differential

expressions of *PFK27*, *ERR3*, *ERR2*, *SOR1*, *YBR242W*, *PDC6*, and *YNL234W* define glycolysis pathway (R-SCE-70171) associated genes (Fig 12B).

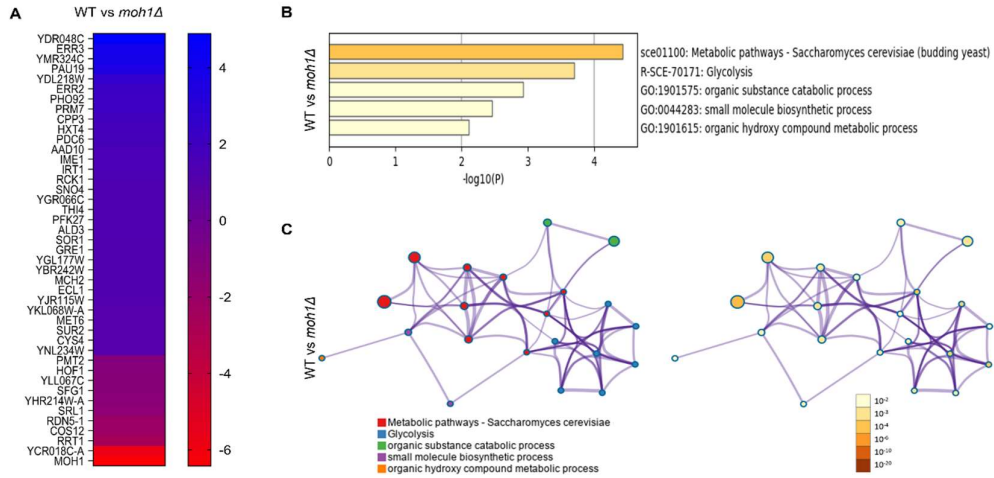


**Figure 12. RNA Seq Results** **A)** Heatmap of differentially expressed genes **B)** Metascape results of differentially expressed genes **C)** A network of enriched terms using differentially expressed genes **D)** The enriched term network is represented by colored p-values

To avoid biases in subsequent analyses due to the small number of genes in pathway enrichments, we also carried out manual annotations using the functional features of each gene product. Results revealed the majority (17/30) of DEG products encompassing *AAD10*, *ALD3*, *CYS4*, *ERR2*, *ERR3*, *GID10*, *MCH2*, *MET6*, *PDC6*, *PFK27*, *PMT2*, *RCK1*, *SNO4*, *SOR1*, *SUR2*, *THI4*, and *YBR242W* are enzymes involved in protein and lipid metabolism, and yeast stress responses. Of the genes, *AAD10*, *ALD3*, *GID10*, *SNO4*, *SUR2*, *THI4*, *CPP3*, *GRE1*, *ECL1*, and *RCK1* are stress-related or pleiotropic stress-responsive genes in *S. Cerevisiae*. *AAD10*, *ALD3*, *SNO4*, *THI4*, *ECL1*, *GRE1*, and *RCK1* are, for example, genes that are oxidative stress-related or oxidative stress-responsive genes [118], [123]-[130]; whereas, *YNL234W*, *ALD3*, *GID10*, *GRE1*, and *THI4* are osmotic stress-related or osmotic stress-induced genes [118], [128], [131]-[133]. Interestingly, the expression of all these stress response genes is upregulated in the *moh1Δ* strain compared to WT cells. This suggests that the absence of *MOH1* in cells leads to the activation of some stress

response genes, which in turn implies that *moh1p* is involved in the stress attenuation in *S. cerevisiae* cells.

Our functional analyses also indicate that some of the stress-responsive DEGs including *AAD10*, *ALD3*, and *SUR2* are also associated with lipid metabolism. *AAD10*, a member of the aryl-alcohol dehydrogenase gene family, encodes for a putative aryl-alcohol dehydrogenase. The expression of *AAD10* is shown to be minimal in cells cultivated under standard aerobic conditions but is elevated under oxygen-limited growth and various stress conditions, including glucose repression, heat shock, osmotic stress, and nitrogen starvation [123], [124], [131]. *ALD3* as cytoplasmic aldehyde dehydrogenase is important for beta-alanine synthesis. The expression of *ALD3* is dependent on the general-stress transcription factors and important for salt stress resistance [118], [119]. Lipid oxidation (lipid peroxidation) is a harmful chain reaction in cell membranes where reactive oxygen species (ROS) oxidize polyunsaturated fatty acids (PUFAs), continuing to damage the membrane until a radical encounters another radical or an antioxidant [134]. Dehydrogenases are important enzymes to cope with this oxidative damage caused by lipid peroxidation. Our FTIR results suggested the degradation of unsaturated and saturated fatty acids in *moh1Δ* cells compared to the WT strain. The main degradation pathway of fatty acids is beta-oxidation [135]. The increase in dehydrogenase expressions indicates an increase in the oxidation of lipids as a result of an oxidative stress response. Sphingolipids are also critical structural components of cell membranes [136], [137]. An increase in the expression of *SUR2*, which is a sphinganine C4-hydroxylase involved in sphingolipid synthesis, in *moh1Δ* cells could indeed contribute to cell survival as *sur2Δ* deletion is shown to be sensitive to oxidative stress [138].

Further analyses reveal that in addition to stress responses, some of the DEGs including *COS12*, *CPP3*, *CYS4*, *GID10*, *MET6*, *PDC6*, *PMT2*, *SNO4*, *PHO92*, and *RDN5* are also involved in protein metabolism. *CYS4*, *PDC6*, *ALD3*, and *MET6* for example play critical roles in amino acid metabolic processes. *CYS4* is cystathionine beta-synthase that catalyzes the conversion of homocysteine as a critical first

committed step in the biosynthesis of cysteine, which is essential for the folding, assembly, and stability of proteins due to its ability to form disulfide bonds [139]. *MET6*, on the other hand, is a cobalamin-independent methionine synthase involved in methionine biosynthesis and regeneration by converting homocysteine into methionine [140]. *MET6* is also important for the synthesis of glutathione (GSH), which protects the cells from oxidative stress [140], [141]. *PDC6* is the minor isoform of pyruvate decarboxylase that decarboxylates pyruvate to acetaldehyde and is also involved in amino acid catabolism [142]. *PDC6* expression is induced under high-glucose stress conditions and its expression is inversely correlated with the oxidation-reduction potential of the cell [120], [143]. Furthermore, some DEGs including *GID10* are involved in protein degradation. *GID10* is a strictly stress-induced gene and encodes a protein as an N-recognin component of the Pro/N-degron pathway that identifies and targets proteins with N-terminal degradation signals for degradation [132], [144]. We also observe that the expression of *PMT2* acting as protein O-mannosyltransferase of the ER membrane which transfers mannose residues from dolichol phosphate-D-mannose to serine/threonine residues of target proteins and is involved in ER protein quality control [145], as well as the expression of *SRL1* which encodes srl1p mannoprotein tightly associated with the cell wall [121] are reduced. These together with a decrease in the transcript levels of *SFG1* acting as a transcription factor for genes encoding cell wall degrading enzymes [146] suggest that the *MOH1* deletion in *S. cerevisiae* leads to an altered state of protein synthesis and degradation which are supportive of our FTIR results.

Collectively these results indicate a correlation between differential gene expressions and biomolecular, including lipids and proteins, modifications that are reflected as structural alterations in the cell wall of *moh1* $\Delta$  cells critical for cell faith in response to various stresses.

## CHAPTER 4

### CONCLUSIONS AND FUTURE DIRECTIONS

Protein functions are closely related to their structural characteristics, and similarities between proteins can be predicted by amino acid homologies. Our *in silico* analyses revealed that:

1. Sequence alignment indicates that human YPEL1-4 proteins have high amino acid sequence homology (83.2-96.6%), whereas YPEL5 is less similar (43.8-49.5%). Moh1p shows 37.8% homology with YPEL2, with lower identity percentages for other YPEL proteins.
2. Both Moh1p and YPEL2 predominantly consist of beta sheets and exhibit globular tertiary structures, with some differences at their amino-terminus regions.
3. Phyre2 analysis indicated that both proteins are related to multiple protein families, including ligases and oxidoreductases, with high confidence.
4. Additionally, functional studies suggest that YPEL2 may be involved in stress response, and Moh1p affects yeast cell survival under stress, implying that Moh1p and YPEL2 could share evolutionary conserved functions.

Our previous studies showed that in the absence of Moh1p, cell survival is affected by various stress conditions differently. Also, studies showed that the *MOH1* gene is essential for cell survival during nutrient-depleted stationary phase conditions, as *moh1Δ* cells cannot endure this phase but show increased viability under various stressors like UV, chemicals, heat, and hyperosmotic shock [22], [32]-[34].

To further investigate Moh1p's functions, particularly concerning oxidative stress, the impact of MOH1 expression was examined under H<sub>2</sub>O<sub>2</sub> stress.

1. RT-qPCR results showed that, MOH1 expression is decreased under short- or long-term oxidative stress induction.
2. When protein levels of the Moh1p are assessed with Western blot, there is a reduction in f-Moh1 protein levels under short- or long-term oxidative stress.

These results suggested that *MOH1* expression and Moh1 protein levels are negatively correlated with oxidative stress exposure.

According to our microscopic observations of the yeast cells, the moh1Δ cells compared to WT have smaller sizes and tend to clump. To understand whether there is a structural or morphological change between moh1Δ cells and WT cells, we used scanning electron microscopy. Our results showed that:

1. WT and moh1Δ-i cells have similar cell sizes and ovoid shapes, whereas moh1Δ cells have a more spherical shape with a rough surface due to protrusions/indentations. This means that moh1Δ cells have different shapes and sizes when compared to WT or moh1Δ-i strains.
2. Also, this shape and size difference are examined under stress conditions. These studies showed that cellular morphology due to Moh1p absence is independent of stress induction with H<sub>2</sub>O<sub>2</sub>.

After morphological studies to understand the underlying cause of morphological differences in MOH1-deleted cells, we performed FTIR. FTIR results revealed that:

1. moh1Δ cells and WT cells have distinct clustering patterns and there is a variation between these cell types according to PCA and HCA plots, indicating differences in the biomolecular content.
2. When lipid content is examined, we find a decrease in unsaturated/saturated fatty acids, whereas the triesterglycerol/cholesterol amount is increased. Also, there is a decrease in membrane fluidity, as the lipid chains are more ordered and more tightly packed.
3. Consistent with changes in lipids, membrane proteins significantly contribute to the regulation of membrane fluidity through lateral mobility, density,

conformational changes as well as interactions with lipids. Protein examinations by FTIR showed that there is a decrease in protein concentration while there is an increase in the conformational changes of proteins in the *moh1Δ* strain compared to the WT cells. In addition to these, protein carbonylation, a common form of protein oxidation, increases dramatically in *moh1Δ* cells.

4. Lastly, since there is a difference in the cell wall of the *moh1Δ* cells and WT cells, beta-glucans and mannans, major cell wall components, were examined. Results indicate that there is a dramatic increase in both beta-glucans and mannan concentrations.

Collectively FTIR results suggest that, in the absence of *MOHI*, the biomolecular composition of cells changes dramatically. Observed changes in membrane permeability and cell wall rigidity might be the cause of the morphological changes in the cell wall.

Lastly, RNA sequencing was performed to understand the transcriptomic changes that occur in the absence of *MOHI*. The RNA-Seq results revealed that:

1. There are 43 differentially expressed genes (DEGs), including *MOHI* as expected, when *moh1Δ* cells compared to the WT cells.
2. Our Metascape and STRING analysis gave a little information about the pathways in which DEGs play a role since the number of DEGs is very small rendering annotation to specific pathways difficult.
3. To understand the importance of DEGs in the cells, we manually annotated DEGs individually. Seventeen of the DEGs are enzymes which are related to protein metabolism, lipid metabolism, and stress response.
4. The increase in the expression of all stress-related genes suggests that the absence of *MOHI* in cells triggers the activation of certain stress response genes. This in turn implies that *Moh1p* plays a role in reducing stress in *S. cerevisiae* cells.

5. DEGs related to lipid metabolism include dehydrogenases and genes that are important for sphingolipid synthesis. Since dehydrogenases decrease the oxidation effects in the cells, an increase in the dehydrogenase expressions could be related to lipid oxidation which may result in a decrease in unsaturated/saturated lipid concentration.
6. Lastly, DEGs related to protein metabolism are associated with amino acid metabolism and protein degradation pathways. Also, there are genes related to cell wall proteins, whose expressions also show decrease. According to these results, MOH1 deletion leads to changes in protein synthesis and protein metabolism which may explain the decrease in protein concentration assessed with FTIR.

Overall, these results suggest that MOH1 deletion leads to morphological changes in yeast cells which is related to changes in the biomolecular composition of the cell and differentially expressed genes which are important for lipid metabolism, protein metabolism, and stress response. This indicates that Moh1p has a crucial role in cell growth under different stress conditions by changing the biomolecular composition and transcriptome of the cells.

To better understand the function of Moh1:

1. TurboID system can be used to find Moh1p protein partners. In cells, proteins function within the context of a dynamically changing network of interacting protein partners. Therefore, deciphering the protein interaction network in cells could reveal important information regarding protein function. TurboID, a proximity-dependent biotin labeling system, is a versatile and effective system to identify the interaction partners of a test protein in the cellular environment [147].
2. Currently, we are working to determine the intracellular localization of MOH1. Proteins operate in the cell within specific subcellular locations to interact with other molecular partners. Therefore, identifying the subcellular localization of a protein can provide insights into its function [148].

3. Proteins are made of amino acid chains that fold into specific three-dimensional shapes. Bonds within the protein help stable confirmation, allowing it to perform its function effectively [149]. Therefore, the structural properties of a protein can give a clue about the protein's function. Therefore, we are planning to decipher the 3D structure of Moh1p by producing Moh1p recombinant protein.



## REFERENCES

- [1] S. L. Nott *et al.*, “Genomic Responses from the Estrogen-responsive Element-dependent Signaling Pathway Mediated by Estrogen Receptor  $\alpha$  Are Required to Elicit Cellular Alterations,” *Journal of Biological Chemistry*, vol. 284, no. 22, pp. 15277–15288, May 2009, doi: 10.1074/jbc.M900365200.
- [2] K. Hosono, T. Sasaki, S. Minoshima, and N. Shimizu, “Identification and characterization of a novel gene family YPEL in a wide spectrum of eukaryotic species,” *Gene*, vol. 340, no. 1, pp. 31–43, Sep. 2004, doi: 10.1016/j.gene.2004.06.014.
- [3] K. Roxström-Lindquist and I. Faye, “The *Drosophila* gene *Yippee* reveals a novel family of putative zinc binding proteins highly conserved among eukaryotes,” *Insect Mol Biol*, vol. 10, no. 1, pp. 77–86, Feb. 2001, doi: 10.1046/j.1365-2583.2001.00239.x.
- [4] K. Hosono *et al.*, “YPEL5 protein of the YPEL gene family is involved in the cell cycle progression by interacting with two distinct proteins RanBPM and RanBP10,” *Genomics*, vol. 96, no. 2, pp. 102–111, Aug. 2010, doi: 10.1016/j.ygeno.2010.05.003.
- [5] G. Gupur, “Cloning and Initial Protein Characterization of an estrogen responsive gene: YPEL2,” Middle East Technical University, 2014.
- [6] S. Aerts *et al.*, “Gene prioritization through genomic data fusion,” *Nat Biotechnol*, vol. 24, no. 6, pp. 719–719, Jun. 2006, doi: 10.1038/nbt0606-719d.
- [7] P. Farlie, C. Reid, S. Wilcox, J. Peeters, G. Reed, and D. Newgreen, “Ypel1: a novel nuclear protein that induces an epithelial-like morphology in fibroblasts,” *Genes to Cells*, vol. 6, no. 7, pp. 619–629, Jul. 2001, doi: 10.1046/j.1365-2443.2001.00445.x.

- [8] T. Y. Tan, C. T. Gordon, K. A. Miller, D. J. Amor, and P. G. Farlie, “*YPEL1* overexpression in early avian craniofacial mesenchyme causes mandibular dysmorphogenesis by up-regulating apoptosis,” *Developmental Dynamics*, vol. 244, no. 8, pp. 1022–1030, Aug. 2015, doi: 10.1002/dvdy.24299.
- [9] S. Ruiz García *et al.*, “Novel dynamics of human mucociliary differentiation revealed by single-cell RNA sequencing of nasal epithelial cultures,” *Development*, vol. 146, no. 20, Oct. 2019, doi: 10.1242/dev.177428.
- [10] W. Li, W. Huang, K. Wu, and Y. Long, “Yippee Like 1 Suppresses Glioma Progression and Serves as a Novel Prognostic Factor,” *Tohoku J Exp Med*, vol. 256, no. 2, pp. 141–150, 2022, doi: 10.1620/tjem.256.141.
- [11] S. J. Baker, “Small unstable apoptotic protein, an apoptosis-associated protein, suppresses proliferation of myeloid cells.,” *Cancer Res*, vol. 63, no. 3, pp. 705–12, Feb. 2003.
- [12] K. D. Kelley, K. R. Miller, A. Todd, A. R. Kelley, R. Tuttle, and S. J. Berberich, “*YPEL3*, a p53-Regulated Gene that Induces Cellular Senescence,” *Cancer Res*, vol. 70, no. 9, pp. 3566–3575, May 2010, doi: 10.1158/0008-5472.CAN-09-3219.
- [13] R. Tuttle, K. R. Miller, J. N. Maiorano, P. M. Termuhlen, Y. Gao, and S. J. Berberich, “Novel senescence associated gene, *YPEL3*, is repressed by estrogen in ER+ mammary tumor cells and required for tamoxifen-induced cellular senescence,” *Int J Cancer*, vol. 130, no. 10, pp. 2291–2299, May 2012, doi: 10.1002/ijc.26239.
- [14] B. Blanco-Sánchez *et al.*, “yippee like 3 (*ypel3*) is a novel gene required for myelinating and perineurial glia development,” *PLoS Genet*, vol. 16, no. 6, p. e1008841, Jun. 2020, doi: 10.1371/journal.pgen.1008841.
- [15] J. Zhang *et al.*, “*YPEL3* suppresses epithelial–mesenchymal transition and metastasis of nasopharyngeal carcinoma cells through the Wnt/ $\beta$ -catenin

- signaling pathway,” *Journal of Experimental & Clinical Cancer Research*, vol. 35, no. 1, p. 109, Dec. 2016, doi: 10.1186/s13046-016-0384-1.
- [16] J. H. Kim *et al.*, “Frameshift mutations of *YPEL3* alter the sensory circuit function in *Drosophila*,” *Dis Model Mech*, vol. 13, no. 6, Jun. 2020, doi: 10.1242/dmm.042390.
- [17] X. Kong, Y. Li, and X. Zhang, “Increased Expression of the *YPEL3* Gene in Human Colonic Adenocarcinoma Tissue and the Effects on Proliferation, Migration, and Invasion of Colonic Adenocarcinoma Cells In Vitro via the Wnt/b-Catenin Signaling Pathway,” *Medical Science Monitor*, vol. 24, pp. 4767–4775, Jul. 2018, doi: 10.12659/MSM.908173.
- [18] P. Liang *et al.*, “MVP interacts with *YPEL4* and inhibits *YPEL4*-mediated activities of the ERK signal pathway,” *Biochemistry and Cell Biology*, vol. 88, no. 3, pp. 445–450, Jun. 2010, doi: 10.1139/O09-166.
- [19] A. Mattebo *et al.*, “Yippee like 4 (*Ypel4*) is essential for normal mouse red blood cell membrane integrity,” *Sci Rep*, vol. 11, no. 1, p. 15898, Aug. 2021, doi: 10.1038/s41598-021-95291-1.
- [20] K. Oki, M. W. Plonczynski, E. P. Gomez-Sanchez, and C. E. Gomez-Sanchez, “*YPEL4* modulates *HAC15* adrenal cell proliferation and is associated with tumor diameter,” *Mol Cell Endocrinol*, vol. 434, pp. 93–98, Oct. 2016, doi: 10.1016/j.mce.2016.06.022.
- [21] D.-Y. Jun, H.-W. Park, and Y.-H. Kim, “Expression of Yippee-Like 5 (*YPEL5*) Gene During Activation of Human Peripheral T Lymphocytes by Immobilized Anti-CD3,” *J Life Sci*, vol. 17, no. 12, pp. 1641–1648, Dec. 2007, doi: 10.5352/JLS.2007.17.12.1641.
- [22] J. Y. Lee, D. Y. Jun, J. E. Park, G. H. Kwon, J.-S. Kim, and Y. H. Kim, “Pro-Apoptotic Role of the Human *YPEL5* Gene Identified by Functional Complementation of a Yeast *moh1* Mutation,” *J Microbiol Biotechnol*, vol. 27, no. 3, pp. 633–643, Mar. 2017, doi: 10.4014/jmb.1610.10045.

- [23] X. Wu, “Up-regulation of YPEL1 and YPEL5 and down-regulation of ITGA2 in erlotinib-treated EGFR-mutant non-small cell lung cancer: A bioinformatic analysis,” *Gene*, vol. 643, pp. 74–82, Feb. 2018, doi: 10.1016/j.gene.2017.12.003.
- [24] S. Li, M. Y. Sun, and X. Su, “MIR-885-5p promotes gastric cancer proliferation and invasion through regulating YPEL1,” *Eur Rev Med Pharmacol Sci*, vol. 23, no. 18, 2019, doi: 10.26355/eurrev\_201909\_19005.
- [25] M. Vysotskiy, X. Zhong, T. W. Miller-Fleming, D. Zhou, N. J. Cox, and L. A. Weiss, “Integration of genetic, transcriptomic, and clinical data provides insight into 16p11.2 and 22q11.2 CNV genes,” *Genome Med*, vol. 13, no. 1, p. 172, Dec. 2021, doi: 10.1186/s13073-021-00972-1.
- [26] R. Tuttle *et al.*, “Senescence-Associated Gene YPEL3 Is Downregulated in Human Colon Tumors,” *Ann Surg Oncol*, vol. 18, no. 6, pp. 1791–1796, Jun. 2011, doi: 10.1245/s10434-011-1558-x.
- [27] Y. Li *et al.*, “Intestinal mucosa-derived DNA methylation signatures in the penetrating intestinal mucosal lesions of Crohn’s disease,” *Sci Rep*, vol. 11, no. 1, p. 9771, May 2021, doi: 10.1038/s41598-021-89087-6.
- [28] S. E. de Bruijn *et al.*, “Structural Variants Create New Topological-Associated Domains and Ectopic Retinal Enhancer-Gene Contact in Dominant Retinitis Pigmentosa,” *The American Journal of Human Genetics*, vol. 107, no. 5, pp. 802–814, Nov. 2020, doi: 10.1016/j.ajhg.2020.09.002.
- [29] F. Mascia *et al.*, “In search of autophagy biomarkers in breast cancer: Receptor status and drug agnostic transcriptional changes during autophagy flux in cell lines,” *PLoS One*, vol. 17, no. 1, p. e0262134, Jan. 2022, doi: 10.1371/journal.pone.0262134.
- [30] G. Turan *et al.*, “Dynamic proximity interaction profiling suggests that <sc>YPEL2</sc> is involved in cellular stress surveillance,” *Protein Science*, vol. 33, no. 2, Feb. 2024, doi: 10.1002/pro.4859.

- [31] S. Mohammadi, B. Saberidokht, S. Subramaniam, and A. Grama, "Scope and limitations of yeast as a model organism for studying human tissue-specific pathways," *BMC Syst Biol*, vol. 9, no. 1, p. 96, Dec. 2015, doi: 10.1186/s12918-015-0253-0.
- [32] M. J. Martinez *et al.*, "Genomic analysis of stationary-phase and exit in *Saccharomyces cerevisiae*: gene expression and identification of novel essential genes.," *Mol Biol Cell*, 2004, doi: 10.1091/mbc.E03-11-0856.
- [33] K. Ashrafi, T. A. Farazi, and J. I. Gordon, "A role for *Saccharomyces cerevisiae* fatty acid activation protein 4 in regulating protein N-myristoylation during entry into stationary phase," *Journal of Biological Chemistry*, 1998, doi: 10.1074/jbc.273.40.25864.
- [34] D. J. Erasmus, G. K. Van Der Merwe, and H. J. J. Van Vuuren, "Genome-wide expression analyses: Metabolic adaptation of *Saccharomyces cerevisiae* to high sugar stress," *FEMS Yeast Res*, 2003, doi: 10.1016/S1567-1356(02)00203-9.
- [35] J. R. Broach, "Nutritional control of growth and development in yeast," 2012. doi: 10.1534/genetics.111.135731.
- [36] K. J. Livak and T. D. Schmittgen, "Analysis of Relative Gene Expression Data Using Real-Time Quantitative PCR and the  $2^{-\Delta\Delta CT}$  Method," *Methods*, vol. 25, no. 4, pp. 402–408, Dec. 2001, doi: 10.1006/meth.2001.1262.
- [37] S. A. Bustin *et al.*, "The MIQE Guidelines: Minimum Information for Publication of Quantitative Real-Time PCR Experiments," *Clin Chem*, vol. 55, no. 4, pp. 611–622, Apr. 2009, doi: 10.1373/clinchem.2008.112797.
- [38] N. Simsek Ozek, "Exploring the *in vitro* potential of royal jelly against glioblastoma and neuroblastoma: impact on cell proliferation, apoptosis, cell cycle, and the biomolecular content," *Analyst*, vol. 149, no. 6, pp. 1872–1884, 2024, doi: 10.1039/D3AN01840G.

- [39] T. Ceylani, H. T. Teker, G. Samgane, and R. Gurbanov, “Intermittent fasting-induced biomolecular modifications in rat tissues detected by ATR-FTIR spectroscopy and machine learning algorithms,” *Anal Biochem*, vol. 654, p. 114825, Oct. 2022, doi: 10.1016/j.ab.2022.114825.
- [40] F.-Y. Zhu *et al.*, “Comparative performance of the BGISEQ-500 and Illumina HiSeq4000 sequencing platforms for transcriptome analysis in plants,” *Plant Methods*, vol. 14, no. 1, p. 69, Dec. 2018, doi: 10.1186/s13007-018-0337-0.
- [41] A. Dobin *et al.*, “STAR: ultrafast universal RNA-seq aligner,” *Bioinformatics*, vol. 29, no. 1, pp. 15–21, Jan. 2013, doi: 10.1093/bioinformatics/bts635.
- [42] Y. Liao, G. K. Smyth, and W. Shi, “featureCounts: an efficient general purpose program for assigning sequence reads to genomic features,” *Bioinformatics*, vol. 30, no. 7, pp. 923–930, Apr. 2014, doi: 10.1093/bioinformatics/btt656.
- [43] M. I. Love, W. Huber, and S. Anders, “Moderated estimation of fold change and dispersion for RNA-seq data with DESeq2,” *Genome Biol*, vol. 15, no. 12, p. 550, Dec. 2014, doi: 10.1186/s13059-014-0550-8.
- [44] F. Morandat, B. Hill, L. Osvald, and J. Vitek, “Evaluating the Design of the R Language,” 2012, pp. 104–131. doi: 10.1007/978-3-642-31057-7\_6.
- [45] Y. Zhou *et al.*, “Metascape provides a biologist-oriented resource for the analysis of systems-level datasets,” *Nat Commun*, vol. 10, no. 1, p. 1523, Apr. 2019, doi: 10.1038/s41467-019-09234-6.
- [46] W. R. Pearson, “An Introduction to Sequence Similarity (‘Homology’) Searching,” *Curr Protoc Bioinformatics*, vol. 42, no. 1, Jun. 2013, doi: 10.1002/0471250953.bi0301s42.
- [47] A. M. Waterhouse, J. B. Procter, D. M. A. Martin, M. Clamp, and G. J. Barton, “Jalview Version 2—a multiple sequence alignment editor and analysis

- workbench,” *Bioinformatics*, vol. 25, no. 9, pp. 1189–1191, May 2009, doi: 10.1093/bioinformatics/btp033.
- [48] F. Sievers and D. G. Higgins, “The Clustal Omega Multiple Alignment Package,” 2021, pp. 3–16. doi: 10.1007/978-1-0716-1036-7\_1.
- [49] A. Drozdetskiy, C. Cole, J. Procter, and G. J. Barton, “JPred4: a protein secondary structure prediction server,” *Nucleic Acids Res*, vol. 43, no. W1, pp. W389–W394, Jul. 2015, doi: 10.1093/nar/gkv332.
- [50] J. Jumper *et al.*, “Highly accurate protein structure prediction with AlphaFold,” *Nature*, vol. 596, no. 7873, pp. 583–589, Aug. 2021, doi: 10.1038/s41586-021-03819-2.
- [51] M. Varadi *et al.*, “AlphaFold Protein Structure Database: massively expanding the structural coverage of protein-sequence space with high-accuracy models,” *Nucleic Acids Res*, vol. 50, no. D1, pp. D439–D444, Jan. 2022, doi: 10.1093/nar/gkab1061.
- [52] E. F. Pettersen *et al.*, “<scp>UCSF ChimeraX</scp> : Structure visualization for researchers, educators, and developers,” *Protein Science*, vol. 30, no. 1, pp. 70–82, Jan. 2021, doi: 10.1002/pro.3943.
- [53] T. D. Goddard *et al.*, “UCSF ChimeraX: Meeting modern challenges in visualization and analysis,” *Protein Science*, vol. 27, no. 1, pp. 14–25, Jan. 2018, doi: 10.1002/pro.3235.
- [54] L. A. Kelley, S. Mezulis, C. M. Yates, M. N. Wass, and M. J. E. Sternberg, “The Phyre2 web portal for protein modeling, prediction and analysis,” *Nat Protoc*, vol. 10, no. 6, pp. 845–858, Jun. 2015, doi: 10.1038/nprot.2015.053.
- [55] E. Cabib, V. Farkas, O. Kosík, N. Blanco, J. Arroyo, and P. McPhie, “Assembly of the Yeast Cell Wall,” *Journal of Biological Chemistry*, vol. 283, no. 44, pp. 29859–29872, Oct. 2008, doi: 10.1074/jbc.M804274200.

- [56] M. Schmidt, J. Z. Schaumberg, C. M. Steen, and M. P. Boyer, “Boric Acid Disturbs Cell Wall Synthesis in *Saccharomyces cerevisiae*,” *Int J Microbiol*, vol. 2010, pp. 1–10, 2010, doi: 10.1155/2010/930465.
- [57] Y. R. Herrero, K. L. Camas, and A. Ullah, “Characterization of biobased materials,” in *Advanced Applications of Biobased Materials*, Elsevier, 2023, pp. 111–143. doi: 10.1016/B978-0-323-91677-6.00005-2.
- [58] S.-Y. Tang, W. Zhang, R. Soffe, S. Nahavandi, R. Shukla, and K. Khoshmanesh, “High Resolution Scanning Electron Microscopy of Cells Using Dielectrophoresis,” *PLoS One*, vol. 9, no. 8, p. e104109, Aug. 2014, doi: 10.1371/journal.pone.0104109.
- [59] C. A. Schneider, W. S. Rasband, and K. W. Eliceiri, “NIH Image to ImageJ: 25 years of image analysis,” *Nat Methods*, vol. 9, no. 7, pp. 671–675, Jul. 2012, doi: 10.1038/nmeth.2089.
- [60] R. Sidari and A. Caridi, “Nutrient depletion modifies cell wall adsorption activity of wine yeast,” *World J Microbiol Biotechnol*, vol. 32, no. 6, p. 89, Jun. 2016, doi: 10.1007/s11274-016-2047-y.
- [61] R. A. Ribeiro, N. Bourbon-Melo, and I. Sá-Correia, “The cell wall and the response and tolerance to stresses of biotechnological relevance in yeasts,” *Front Microbiol*, vol. 13, Jul. 2022, doi: 10.3389/fmicb.2022.953479.
- [62] P. N. Lipke and R. Ovalle, “Cell Wall Architecture in Yeast: New Structure and New Challenges,” *J Bacteriol*, vol. 180, no. 15, pp. 3735–3740, Aug. 1998, doi: 10.1128/JB.180.15.3735-3740.1998.
- [63] G. Lesage and H. Bussey, “Cell Wall Assembly in *Saccharomyces cerevisiae*,” *Microbiology and Molecular Biology Reviews*, vol. 70, no. 2, pp. 317–343, Jun. 2006, doi: 10.1128/MMBR.00038-05.

- [64] J. Ruiz-Herrera and L. Ortiz-Castellanos, “Cell wall glucans of fungi. A review,” *The Cell Surface*, vol. 5, p. 100022, Dec. 2019, doi: 10.1016/j.tcs.2019.100022.
- [65] G. G. Stewart, “The Structure and Function of the Yeast Cell Wall, Plasma Membrane and Periplasm,” in *Brewing and Distilling Yeasts*, Cham: Springer International Publishing, 2017, pp. 55–75. doi: 10.1007/978-3-319-69126-8\_5.
- [66] M. E. van der Rest, A. H. Kamminga, A. Nakano, Y. Anraku, B. Poolman, and W. N. Konings, “The plasma membrane of *Saccharomyces cerevisiae*: structure, function, and biogenesis,” *Microbiol Rev*, vol. 59, no. 2, pp. 304–322, Jun. 1995, doi: 10.1128/mr.59.2.304-322.1995.
- [67] L. Klug and G. Daum, “Yeast lipid metabolism at a glance,” *FEMS Yeast Res*, vol. 14, no. 3, pp. 369–388, May 2014, doi: 10.1111/1567-1364.12141.
- [68] D. J. Montefusco, N. Matmati, and Y. A. Hannun, “The yeast sphingolipid signaling landscape,” *Chem Phys Lipids*, vol. 177, pp. 26–40, Jan. 2014, doi: 10.1016/j.chemphyslip.2013.10.006.
- [69] R. F. M. de Almeida, “A route to understanding yeast cellular envelope – plasma membrane lipids interplaying in cell wall integrity,” *FEBS J*, vol. 285, no. 13, pp. 2402–2404, Jul. 2018, doi: 10.1111/febs.14526.
- [70] E. Knözinger, “P. R. Griffiths, J. A. de Haseth: Fourier Transform Infrared Spectroscopy, Vol. 83 aus der Reihe: Chemical Analysis—A Series of Monographs of Analytical Chemistry and Its Applications, John Wiley + Sons, Chichester, New York, Brisbane, Toronto, Singapore 1986. 656 Seiten, Preis: £ 76.75.,” *Berichte der Bunsengesellschaft für physikalische Chemie*, vol. 90, no. 12, pp. 1240–1241, Dec. 1986, doi: 10.1002/bbpc.19860901224.
- [71] V. Erukhimovitch, M. Karpasasa, and M. Huleihel, “Spectroscopic detection and identification of infected cells with herpes viruses,” *Biopolymers*, vol. 91, no. 1, pp. 61–67, Jan. 2009, doi: 10.1002/bip.21082.

- [72] P. Lasch and J. Kneipp, Eds., *Biomedical Vibrational Spectroscopy*. Wiley, 2008. doi: 10.1002/9780470283172.
- [73] E. Taillandier and J. Liquier, “[16] Infrared spectroscopy of DNA,” 1992, pp. 307–335. doi: 10.1016/0076-6879(92)11018-E.
- [74] W. K. Surewicz and H. H. Mantsch, “New insight into protein secondary structure from resolution-enhanced infrared spectra,” *Biochimica et Biophysica Acta (BBA) - Protein Structure and Molecular Enzymology*, vol. 952, pp. 115–130, Jan. 1988, doi: 10.1016/0167-4838(88)90107-0.
- [75] H. H. Mantsch and R. N. McElhaney, “Phospholipid phase transitions in model and biological membranes as studied by infrared spectroscopy,” *Chem Phys Lipids*, vol. 57, no. 2–3, pp. 213–226, Mar. 1991, doi: 10.1016/0009-3084(91)90077-O.
- [76] L. CHOO, M. JACKSON, W. HALLIDAY, and H. MANTSCH, “Infrared spectroscopic characterisation of multiple sclerosis plaques in the human central nervous system,” *Biochimica et Biophysica Acta (BBA) - Molecular Basis of Disease*, vol. 1182, no. 3, pp. 333–337, Oct. 1993, doi: 10.1016/0925-4439(93)90078-F.
- [77] D. Naumann, D. Helm, and H. Labischinski, “Microbiological characterizations by FT-IR spectroscopy,” *Nature*, vol. 351, no. 6321, pp. 81–82, May 1991, doi: 10.1038/351081a0.
- [78] D. Helm, H. Labischinski, G. Schallehn, and D. Naumann, “Classification and identification of bacteria by Fourier-transform infrared spectroscopy,” *Microbiology (N Y)*, vol. 137, no. 1, pp. 69–79, Jan. 1991, doi: 10.1099/00221287-137-1-69.
- [79] L. Corte, P. Rellini, L. Roscini, F. Fatichenti, and G. Cardinali, “Development of a novel, FTIR (Fourier transform infrared spectroscopy) based, yeast bioassay for toxicity testing and stress response study,” *Anal Chim Acta*, vol. 659, no. 1–2, pp. 258–265, Feb. 2010, doi: 10.1016/j.aca.2009.11.035.

- [80] W. Mihoubi, E. Sahli, A. Gargouri, and C. Amiel, “FTIR spectroscopy of whole cells for the monitoring of yeast apoptosis mediated by p53 over-expression and its suppression by *Nigella sativa* extracts,” *PLoS One*, vol. 12, no. 7, p. e0180680, Jul. 2017, doi: 10.1371/journal.pone.0180680.
- [81] M. Taha, M. Hassan, S. Essa, and Y. Tartor, “Use of Fourier transform infrared spectroscopy (FTIR) spectroscopy for rapid and accurate identification of Yeasts isolated from human and animals,” *Int J Vet Sci Med*, vol. 1, no. 1, pp. 15–20, Jun. 2013, doi: 10.1016/j.ijvsm.2013.03.001.
- [82] V. Shapaval *et al.*, “Biochemical profiling, prediction of total lipid content and fatty acid profile in oleaginous yeasts by FTIR spectroscopy,” *Biotechnol Biofuels*, vol. 12, no. 1, p. 140, Dec. 2019, doi: 10.1186/s13068-019-1481-0.
- [83] M. Kümmerle, S. Scherer, and H. Seiler, “Rapid and Reliable Identification of Food-Borne Yeasts by Fourier-Transform Infrared Spectroscopy,” *Appl Environ Microbiol*, vol. 64, no. 6, pp. 2207–2214, Jun. 1998, doi: 10.1128/AEM.64.6.2207-2214.1998.
- [84] M. Cavagna, R. Dell’Anna, F. Monti, F. Rossi, and S. Torriani, “Use of ATR-FTIR Microspectroscopy to Monitor Autolysis of *Saccharomyces cerevisiae* Cells in a Base Wine,” *J Agric Food Chem*, vol. 58, no. 1, pp. 39–45, Jan. 2010, doi: 10.1021/jf902369s.
- [85] L. Corte, L. Antonielli, L. Roscini, F. Fatichenti, and G. Cardinali, “Influence of cell parameters in Fourier transform infrared spectroscopy analysis of whole yeast cells,” *Analyst*, vol. 136, no. 11, p. 2339, 2011, doi: 10.1039/c0an00515k.
- [86] S. Correa-García, M. Bermúdez-Moretti, A. Travo, G. Déléris, and I. Forfar, “FTIR spectroscopic metabolome analysis of lyophilized and fresh *Saccharomyces cerevisiae* yeast cells,” *Analytical Methods*, vol. 6, no. 6, p. 1855, 2014, doi: 10.1039/c3ay42322k.

- [87] V. Shapaval *et al.*, “FTIR spectroscopic characterization of differently cultivated food related yeasts,” *Analyst*, vol. 138, no. 14, p. 4129, 2013, doi: 10.1039/c3an00304c.
- [88] A. Rohman, A. Windarsih, E. Lukitaningsih, M. Rafi, K. Betania, and N. A. Fadzillah, “The use of FTIR and Raman spectroscopy in combination with chemometrics for analysis of biomolecules in biomedical fluids: A review,” *Biomed Spectrosc Imaging*, vol. 8, no. 3–4, pp. 55–71, Jan. 2020, doi: 10.3233/BSI-200189.
- [89] V. G. Franco, J. C. Perín, V. E. Mantovani, and H. C. Goicoechea, “Monitoring substrate and products in a bioprocess with FTIR spectroscopy coupled to artificial neural networks enhanced with a genetic-algorithm-based method for wavelength selection,” *Talanta*, vol. 68, no. 3, pp. 1005–1012, Jan. 2006, doi: 10.1016/j.talanta.2005.07.003.
- [90] A. Stöbener, U. Naefken, J. Kleber, and A. Liese, “Determination of trace amounts with ATR FTIR spectroscopy and chemometrics: 5-(hydroxymethyl)furfural in honey,” *Talanta*, vol. 204, pp. 1–5, Nov. 2019, doi: 10.1016/j.talanta.2019.05.092.
- [91] H. Wagner, Z. Liu, U. Langner, K. Stehfest, and C. Wilhelm, “The use of FTIR spectroscopy to assess quantitative changes in the biochemical composition of microalgae,” *J Biophotonics*, vol. 3, no. 8–9, pp. 557–566, Aug. 2010, doi: 10.1002/jbio.201000019.
- [92] R. Jamwal *et al.*, “Rapid and non-destructive approach for the detection of fried mustard oil adulteration in pure mustard oil via ATR-FTIR spectroscopy-chemometrics,” *Spectrochim Acta A Mol Biomol Spectrosc*, vol. 244, p. 118822, Jan. 2021, doi: 10.1016/j.saa.2020.118822.
- [93] A. Fernández-González, Á. J. Obaya, C. Chimeno-Trinchet, T. Fontanil, and R. Badía-Laíño, “Viability of ABO Blood Typing with ATR-FTIR

- Spectroscopy,” *Applied Sciences*, vol. 13, no. 17, p. 9650, Aug. 2023, doi: 10.3390/app13179650.
- [94] T. Hasegawa, “Chemometrics for FTIR,” in *Quantitative Infrared Spectroscopy for Understanding of a Condensed Matter*, Tokyo: Springer Japan, 2017, pp. 127–163. doi: 10.1007/978-4-431-56493-5\_5.
- [95] R. Jamwal *et al.*, “Attenuated total Reflectance–Fourier transform infrared (ATR–FTIR) spectroscopy coupled with chemometrics for rapid detection of argemone oil adulteration in mustard oil,” *LWT*, vol. 120, p. 108945, Feb. 2020, doi: 10.1016/j.lwt.2019.108945.
- [96] A. Ghosh, S. Raha, S. Dey, K. Chatterjee, A. Roy Chowdhury, and A. Barui, “Chemometric analysis of integrated FTIR and Raman spectra obtained by non-invasive exfoliative cytology for the screening of oral cancer,” *Analyst*, vol. 144, no. 4, pp. 1309–1325, 2019, doi: 10.1039/C8AN02092B.
- [97] H. Vardin, A. Tay, B. Ozen, and L. Mauer, “Authentication of pomegranate juice concentrate using FTIR spectroscopy and chemometrics,” *Food Chem*, vol. 108, no. 2, pp. 742–748, May 2008, doi: 10.1016/j.foodchem.2007.11.027.
- [98] H. Abdi and L. J. Williams, “Principal component analysis,” *WIREs Computational Statistics*, vol. 2, no. 4, pp. 433–459, Jul. 2010, doi: 10.1002/wics.101.
- [99] H. Grahn, N. M. Szeverenyi, M. W. Roggenbuck, F. Delaglio, and P. Geladi, “Data analysis of multivariate magnetic resonance images I. A principal component analysis approach,” *Chemometrics and Intelligent Laboratory Systems*, vol. 5, no. 4, pp. 311–322, Apr. 1989, doi: 10.1016/0169-7439(89)80030-9.
- [100] J. R. Beattie and F. W. L. Esmonde-White, “Exploration of Principal Component Analysis: Deriving Principal Component Analysis Visually

- Using Spectra,” *Appl Spectrosc*, vol. 75, no. 4, pp. 361–375, Apr. 2021, doi: 10.1177/0003702820987847.
- [101] D. Cozzolino, A. Power, and J. Chapman, “Interpreting and Reporting Principal Component Analysis in Food Science Analysis and Beyond,” *Food Anal Methods*, vol. 12, no. 11, pp. 2469–2473, Nov. 2019, doi: 10.1007/s12161-019-01605-5.
- [102] X. Liu, C. M. G. C. Renard, S. Bureau, and C. Le Bourvellec, “Revisiting the contribution of ATR-FTIR spectroscopy to characterize plant cell wall polysaccharides,” *Carbohydr Polym*, vol. 262, p. 117935, Jun. 2021, doi: 10.1016/j.carbpol.2021.117935.
- [103] H. Köhn and L. J. Hubert, “Hierarchical Cluster Analysis,” in *Wiley StatsRef: Statistics Reference Online*, Wiley, 2015, pp. 1–13. doi: 10.1002/9781118445112.stat02449.pub2.
- [104] D. R. Whelan, K. R. Bambery, L. Puskar, D. McNaughton, and B. R. Wood, “Synchrotron Fourier transform infrared (FTIR) analysis of single living cells progressing through the cell cycle,” *Analyst*, vol. 138, no. 14, p. 3891, 2013, doi: 10.1039/c3an00316g.
- [105] E. Goormaghtigh, J.-M. Ruyschaert, and V. Raussens, “Evaluation of the Information Content in Infrared Spectra for Protein Secondary Structure Determination,” *Biophys J*, vol. 90, no. 8, pp. 2946–2957, Apr. 2006, doi: 10.1529/biophysj.105.072017.
- [106] D. Ami, R. Posterl, P. Mereghetti, D. Porro, S. M. Doglia, and P. Branduardi, “Fourier transform infrared spectroscopy as a method to study lipid accumulation in oleaginous yeasts,” *Biotechnol Biofuels*, vol. 7, no. 1, p. 12, Dec. 2014, doi: 10.1186/1754-6834-7-12.
- [107] G. Socrates, *Infrared and Raman characteristic group frequencies: tables and charts*, 3rd ed. 2001.

- [108] A. Kassem *et al.*, “Applications of Fourier Transform-Infrared spectroscopy in microbial cell biology and environmental microbiology: advances, challenges, and future perspectives,” *Front Microbiol*, vol. 14, Nov. 2023, doi: 10.3389/fmicb.2023.1304081.
- [109] K. A. Oberg, J. Ruyschaert, and E. Goormaghtigh, “The optimization of protein secondary structure determination with infrared and circular dichroism spectra,” *Eur J Biochem*, vol. 271, no. 14, pp. 2937–2948, Jul. 2004, doi: 10.1111/j.1432-1033.2004.04220.x.
- [110] S. Pebotuwa, K. Kochan, A. Peleg, B. R. Wood, and P. Heraud, “Influence of the Sample Preparation Method in Discriminating *Candida* spp. Using ATR-FTIR Spectroscopy,” *Molecules*, vol. 25, no. 7, p. 1551, Mar. 2020, doi: 10.3390/molecules25071551.
- [111] A. Galichet, G. D. Sockalingum, A. Belarbi, and M. Manfait, “FTIR spectroscopic analysis of *Saccharomyces cerevisiae* cell walls: study of an anomalous strain exhibiting a pink-colored cell phenotype,” *FEMS Microbiol Lett*, vol. 197, no. 2, pp. 179–186, Apr. 2001, doi: 10.1111/j.1574-6968.2001.tb10601.x.
- [112] S. Garip, F. Bozoglu, and F. Severcan, “Differentiation of Mesophilic and Thermophilic Bacteria with Fourier Transform Infrared Spectroscopy,” *Appl Spectrosc*, vol. 61, no. 2, pp. 186–192, Feb. 2007, doi: 10.1366/000370207779947486.
- [113] Y. Lu and J. Guo, “Metal-ion interactions with sugars. Crystal structure and FT-IR study of PrCl<sub>3</sub>-d-ribose complex,” *Carbohydr Res*, vol. 341, no. 5, pp. 683–687, Apr. 2006, doi: 10.1016/j.carres.2005.12.011.
- [114] D. A. Los and N. Murata, “Membrane fluidity and its roles in the perception of environmental signals,” *Biochimica et Biophysica Acta (BBA) - Biomembranes*, vol. 1666, no. 1–2, pp. 142–157, Nov. 2004, doi: 10.1016/j.bbamem.2004.08.002.

- [115] C. Laroche, L. Beney, P. A. Marechal, and P. Gervais, “The effect of osmotic pressure on the membrane fluidity of *Saccharomyces cerevisiae* at different physiological temperatures,” *Appl Microbiol Biotechnol*, vol. 56, no. 1–2, pp. 249–254, Jul. 2001, doi: 10.1007/s002530000583.
- [116] Y. Yang *et al.*, “Membrane Fluidity of *Saccharomyces cerevisiae* from *Huangjiu* (Chinese Rice Wine) Is Variably Regulated by *OLE1* To Offset the Disruptive Effect of Ethanol,” *Appl Environ Microbiol*, vol. 85, no. 23, Dec. 2019, doi: 10.1128/AEM.01620-19.
- [117] T. Nyström, “Role of oxidative carbonylation in protein quality control and senescence,” *EMBO J*, vol. 24, no. 7, pp. 1311–1317, Apr. 2005, doi: 10.1038/sj.emboj.7600599.
- [118] J. P. Navarro-Aviño, R. Prasad, V. J. Miralles, R. M. Benito, and R. Serrano, “A proposal for nomenclature of aldehyde dehydrogenases in *Saccharomyces cerevisiae* and characterization of the stress-inducible *ALD2* and *ALD3* genes,” *Yeast*, vol. 15, no. 10A, pp. 829–842, Jul. 1999, doi: 10.1002/(SICI)1097-0061(199907)15:10A<829::AID-YEA423>3.0.CO;2-9.
- [119] W. H. White, P. L. Skatrud, Z. Xue, and J. H. Toyn, “Specialization of Function Among Aldehyde Dehydrogenases: The *ALD2* and *ALD3* Genes Are Required for  $\beta$ -Alanine Biosynthesis in *Saccharomyces cerevisiae*,” *Genetics*, vol. 163, no. 1, pp. 69–77, Jan. 2003, doi: 10.1093/genetics/163.1.69.
- [120] D. ERASMUS, G. VANDERMERWE, and H. VANVUUREN, “Genome-wide expression analyses: Metabolic adaptation of to high sugar stress,” *FEMS Yeast Res*, vol. 3, no. 4, pp. 375–399, Jun. 2003, doi: 10.1016/S1567-1356(02)00203-9.
- [121] I. Hagen *et al.*, “*Sed1p* and *Srl1p* are required to compensate for cell wall instability in *Saccharomyces cerevisiae* mutants defective in multiple GPI-anchored mannoproteins,” *Mol Microbiol*, vol. 52, no. 5, pp. 1413–1425, Jun. 2004, doi: 10.1111/j.1365-2958.2004.04064.x.

- [122] D. Szklarczyk *et al.*, “STRING v11: protein–protein association networks with increased coverage, supporting functional discovery in genome-wide experimental datasets,” *Nucleic Acids Res*, vol. 47, no. D1, pp. D607–D613, Jan. 2019, doi: 10.1093/nar/gky1131.
- [123] H. Iwahashi *et al.*, “Evaluation of toxicity of the mycotoxin citrinin using yeast ORF DNA microarray and Oligo DNA microarray,” *BMC Genomics*, vol. 8, no. 1, p. 95, 2007, doi: 10.1186/1471-2164-8-95.
- [124] D.-D. Yang, G. M. de Billerbeck, J. Zhang, F. Rosenzweig, and J.-M. Francois, “Deciphering the Origin, Evolution, and Physiological Function of the Subtelomeric Aryl-Alcohol Dehydrogenase Gene Family in the Yeast *Saccharomyces cerevisiae*,” *Appl Environ Microbiol*, vol. 84, no. 1, Jan. 2018, doi: 10.1128/AEM.01553-17.
- [125] J. Adameczyk *et al.*, “Copy number variations of genes involved in stress responses reflect the redox state and DNA damage in brewing yeasts,” *Cell Stress Chaperones*, vol. 21, no. 5, pp. 849–864, Sep. 2016, doi: 10.1007/s12192-016-0710-8.
- [126] L. Miller-Fleming, P. Antas, T. F. Pais, J. L. Smalley, F. Giorgini, and T. F. Outeiro, “Yeast DJ-1 superfamily members are required for diauxic-shift reprogramming and cell survival in stationary phase,” *Proceedings of the National Academy of Sciences*, vol. 111, no. 19, pp. 7012–7017, May 2014, doi: 10.1073/pnas.1319221111.
- [127] R. Medina-Silva, M. P. Barros, R. S. Galhardo, L. E. S. Netto, P. Colepicolo, and C. F. M. Menck, “Heat stress promotes mitochondrial instability and oxidative responses in yeast deficient in thiazole biosynthesis,” *Res Microbiol*, vol. 157, no. 3, pp. 275–281, Apr. 2006, doi: 10.1016/j.resmic.2005.07.004.
- [128] A. Garay-Arroyo and A. A. Covarrubias, “Three genes whose expression is induced by stress in *Saccharomyces cerevisiae*,” *Yeast*, vol. 15, no. 10A, pp.

879–892, Jul. 1999, doi: 10.1002/(SICI)1097-0061(199907)15:10A<879::AID-YEA428>3.0.CO;2-Q.

- [129] E. Bilslund, C. Molin, S. Swaminathan, A. Ramne, and P. Sunnerhagen, “Rck1 and Rck2 MAPKAP kinases and the HOG pathway are required for oxidative stress resistance,” *Mol Microbiol*, vol. 53, no. 6, pp. 1743–1756, Sep. 2004, doi: 10.1111/j.1365-2958.2004.04238.x.
- [130] K. AZUMA, H. OHTSUKA, S. MITA, H. MURAKAMI, and H. AIBA, “Identification and Characterization of an Ecl1-Family Gene in *Saccharomyces cerevisiae*,” *Biosci Biotechnol Biochem*, vol. 73, no. 12, pp. 2787–2789, Dec. 2009, doi: 10.1271/bbb.90599.
- [131] G. Sartori *et al.*, “Characterization of a New Hemoprotein in the Yeast *Saccharomyces cerevisiae*,” *Journal of Biological Chemistry*, vol. 274, no. 8, pp. 5032–5037, Feb. 1999, doi: 10.1074/jbc.274.8.5032.
- [132] A. Melnykov, S.-J. Chen, and A. Varshavsky, “Gid10 as an alternative N-recognin of the Pro/N-degron pathway,” *Proceedings of the National Academy of Sciences*, vol. 116, no. 32, pp. 15914–15923, Aug. 2019, doi: 10.1073/pnas.1908304116.
- [133] X. Shi, Y. Zou, Y. Chen, and H. Ying, “Overexpression of THI4 and HAP4 Improves Glucose Metabolism and Ethanol Production in *Saccharomyces cerevisiae*,” *Front Microbiol*, vol. 9, Jun. 2018, doi: 10.3389/fmicb.2018.01444.
- [134] F. T. E. Alban, D. Gyamfi, R. F. van Golen, and M. Heger, “Reactive Oxygen and Nitrogen Species and Liver Ischemia-Reperfusion Injury: An Overview,” in *The Liver*, Elsevier, 2018, pp. 79–96. doi: 10.1016/B978-0-12-803951-9.00008-2.
- [135] G. Litwack, “Metabolism of Fat, Carbohydrate, and Nucleic Acids,” in *Human Biochemistry*, Elsevier, 2022, pp. 441–474. doi: 10.1016/B978-0-323-85718-5.00002-9.

- [136] L. M. Obeid, Y. Okamoto, and C. Mao, “Yeast sphingolipids: metabolism and biology,” *Biochimica et Biophysica Acta (BBA) - Molecular and Cell Biology of Lipids*, vol. 1585, no. 2–3, pp. 163–171, Dec. 2002, doi: 10.1016/S1388-1981(02)00337-2.
- [137] G. M. Jenkins, A. Richards, T. Wahl, C. Mao, L. Obeid, and Y. Hannun, “Involvement of Yeast Sphingolipids in the Heat Stress Response of *Saccharomyces cerevisiae*,” *Journal of Biological Chemistry*, vol. 272, no. 51, pp. 32566–32572, Dec. 1997, doi: 10.1074/jbc.272.51.32566.
- [138] D. J. Montefusco, N. Matmati, and Y. A. Hannun, “The yeast sphingolipid signaling landscape,” *Chem Phys Lipids*, vol. 177, pp. 26–40, Jan. 2014, doi: 10.1016/j.chemphyslip.2013.10.006.
- [139] H. M. Blank, S. Gajjar, A. Belyanin, and M. Polymenis, “Sulfur Metabolism Actively Promotes Initiation of Cell Division in Yeast,” *PLoS One*, vol. 4, no. 11, p. e8018, Nov. 2009, doi: 10.1371/journal.pone.0008018.
- [140] H. Takagi, “Metabolic regulatory mechanisms and physiological roles of functional amino acids and their applications in yeast,” *Biosci Biotechnol Biochem*, vol. 83, no. 8, pp. 1449–1462, Aug. 2019, doi: 10.1080/09168451.2019.1576500.
- [141] X. Yu and Y. C. Long, “Crosstalk between cystine and glutathione is critical for the regulation of amino acid signaling pathways and ferroptosis,” *Sci Rep*, vol. 6, no. 1, p. 30033, Jul. 2016, doi: 10.1038/srep30033.
- [142] J. R. Dickinson, L. E. J. Salgado, and M. J. E. Hewlins, “The Catabolism of Amino Acids to Long Chain and Complex Alcohols in *Saccharomyces cerevisiae*,” *Journal of Biological Chemistry*, vol. 278, no. 10, pp. 8028–8034, Mar. 2003, doi: 10.1074/jbc.M211914200.
- [143] C. Liu, Y. Lin, and F. Bai, “Global gene expression analysis of *Saccharomyces cerevisiae* grown under redox potential-controlled very-high-

- gravity conditions,” *Biotechnol J*, vol. 8, no. 11, pp. 1332–1340, Nov. 2013, doi: 10.1002/biot.201300127.
- [144] J. Regelman *et al.*, “Catabolite Degradation of Fructose-1,6-bisphosphatase in the Yeast *Saccharomyces cerevisiae*: A Genome-wide Screen Identifies Eight Novel *GID* Genes and Indicates the Existence of Two Degradation Pathways,” *Mol Biol Cell*, vol. 14, no. 4, pp. 1652–1663, Apr. 2003, doi: 10.1091/mbc.e02-08-0456.
- [145] M. Lussier, M. Gentzsch, A.-M. Sdicu, H. Bussey, and W. Tanner, “Protein O-Glycosylation in Yeast,” *Journal of Biological Chemistry*, vol. 270, no. 6, pp. 2770–2775, Feb. 1995, doi: 10.1074/jbc.270.6.2770.
- [146] A. Fujita, T. Hiroko, F. Hiroko, and C. Oka, “Enhancement of superficial pseudohyphal growth by overexpression of the SFG1 gene in yeast *Saccharomyces cerevisiae*,” *Gene*, vol. 363, pp. 97–104, Dec. 2005, doi: 10.1016/j.gene.2005.06.036.
- [147] T. C. Branon *et al.*, “Efficient proximity labeling in living cells and organisms with TurboID,” *Nat Biotechnol*, vol. 36, no. 9, pp. 880–887, Oct. 2018, doi: 10.1038/nbt.4201.
- [148] M. S. Scott, S. J. Calafell, D. Y. Thomas, and M. T. Hallett, “Refining Protein Subcellular Localization,” *PLoS Comput Biol*, vol. 1, no. 6, p. e66, Nov. 2005, doi: 10.1371/journal.pcbi.0010066.
- [149] B. Alberts, A. Johnson, J. Lewis, M. Raff, K. Roberts, and P. Walter, *Molecular Biology of the Cell*, 4th ed. 2002.

## APPENDICES

### A. PRIMER LIST

**Table 3.** Primers that are used in this study

<b>Primer Name</b>	<b>Sequences (5'-3')</b>
MOH1_qPCR FP	GTTATTCCACTCTCAGCATCGATCGC
MOH1_qPCR REP	CACAGACTAAGTAGTCGCCAGTCAAC
FCY1_qPCR FP	AAGTGTTCTCGGTCGTGGTC
FCY1_qPCR REP	GCATGGAGACAGCGTCGTAT
ALG9_qPCR FP	CACGGATAGTGGCTTTGGTGAACAATTAC
ALG9_qPCR REP	TATGATTATCTGGCAGCAGGAAAGAACTTGGG
ALD3_qPCR FP	CCTGGTTATGGTTCCGTTGTG
ALD3_qPCR REP	CAATACTGAGCCGCCAACCT
GRE1_qPCR FP	TCCCTACGGCGAAGAAAACC
GRE1_qPCR REP	TCGTCGTCCAACCTGACCTTG
SRL1_qPCR FP	ACTACCACTTTAGCGCCCAG
SRL1_qPCR REP	CGCATTGGTAATGGTGGCTG



## B. MIQE CHECKLIST

**Table 4.** MIQE Checklist

ITEM TO CHECK	IMPORTANCE	CHECKLIST
<b>EXPERIMENTAL DESIGN</b>		
Definition of experimental and control groups	<b>E</b>	YES
Number within each group	<b>E</b>	YES
Assay carried out by core lab or investigator's lab?	<b>D</b>	YES
Acknowledgement of authors' contributions	<b>D</b>	N/A
<b>SAMPLE</b>		
Description	<b>E</b>	N/A
Volume/mass of sample processed	<b>D</b>	N/A
Microdissection or macrodissection	<b>E</b>	N/A
Processing procedure	<b>E</b>	N/A
If frozen - how and how quickly?	<b>E</b>	N/A
If fixed - with what, how quickly?	<b>E</b>	N/A
Sample storage conditions and duration (especially for FFPE samples)	<b>E</b>	N/A
<b>NUCLEIC ACID EXTRACTION</b>		
Procedure and/or instrumentation	<b>E</b>	YES
Name of kit and details of any modifications	<b>E</b>	YES
Source of additional reagents used	<b>D</b>	N/A
Details of DNase or RNase treatment	<b>E</b>	YES
Contamination assessment (DNA or RNA)	<b>E</b>	YES
Nucleic acid quantification	<b>E</b>	YES
Instrument and method	<b>E</b>	YES
Purity (A260/A280)	<b>D</b>	NO
Yield	<b>D</b>	NO
RNA integrity method/instrument	<b>E</b>	NO
RIN/RQI or Cq of 3' and 5' transcripts	<b>E</b>	NO
Electrophoresis traces	<b>D</b>	NO
Inhibition testing (Cq dilutions, spike or other)	<b>E</b>	NO

**Table 4.** (Continued)

<b>REVERSE TRANSCRIPTION</b>		
Complete reaction conditions	<b>E</b>	YES
Amount of RNA and reaction volume	<b>E</b>	YES
Priming oligonucleotide (if using GSP) and concentration	<b>E</b>	YES
Reverse transcriptase and concentration	<b>E</b>	YES
Temperature and time	<b>E</b>	YES
Manufacturer of reagents and catalogue numbers	<b>D</b>	YES
Cqs with and without RT	<b>D*</b>	NO
Storage conditions of cDNA	<b>D</b>	YES
<b>qPCR TARGET INFORMATION</b>		
If multiplex, efficiency and LOD of each assay.	<b>E</b>	N/A
Sequence accession number	<b>E</b>	YES
Location of amplicon	<b>D</b>	YES
Amplicon length	<b>E</b>	YES
<i>In silico</i> specificity screen (BLAST, etc)	<b>E</b>	YES
Pseudogenes, retropseudogenes or other homologs?	<b>D</b>	YES
Sequence alignment	<b>D</b>	YES
Secondary structure analysis of amplicon	<b>D</b>	NO
Location of each primer by exon or intron (if applicable)	<b>E</b>	YES
What splice variants are targeted?	<b>E</b>	YES
<b>qPCR OLIGONUCLEOTIDES</b>		
Primer sequences	<b>E</b>	YES
RTPrimerDB Identification Number	<b>D</b>	N/A
Probe sequences	<b>D**</b>	N/A
Location and identity of any modifications	<b>E</b>	N/A
Manufacturer of oligonucleotides	<b>D</b>	YES
Purification method	<b>D</b>	YES

**Table 4.** (Continued)

<b>qPCR PROTOCOL</b>		
Complete reaction conditions	<b>E</b>	YES
Reaction volume and amount of cDNA/DNA	<b>E</b>	N/A
Primer, (probe), Mg <sup>++</sup> and dNTP concentrations	<b>E</b>	N/A
Polymerase identity and concentration	<b>E</b>	YES
Buffer/kit identity and manufacturer	<b>E</b>	YES
Exact chemical constitution of the buffer	<b>D</b>	YES
Additives (SYBR Green I, DMSO, etc.)	<b>E</b>	YES
Manufacturer of plates/tubes and catalog number	<b>D</b>	YES
Complete thermocycling parameters	<b>E</b>	YES
Reaction setup (manual/robotic)	<b>D</b>	YES
Manufacturer of qPCR instrument	<b>E</b>	YES
<b>qPCR VALIDATION</b>		
Evidence of optimisation (from gradients)	<b>D</b>	NO
Specificity (gel, sequence, melt, or digest)	<b>E</b>	YES
For SYBR Green I, C <sub>q</sub> of the NTC	<b>E</b>	YES
Standard curves with slope and y-intercept	<b>E</b>	YES
PCR efficiency calculated from slope	<b>E</b>	YES
Confidence interval for PCR efficiency or standard error	<b>D</b>	NO
r <sup>2</sup> of standard curve	<b>E</b>	YES
Linear dynamic range	<b>E</b>	YES
C <sub>q</sub> variation at lower limit	<b>E</b>	YES
Confidence intervals throughout range	<b>D</b>	N/A
Evidence for limit of detection	<b>E</b>	NO
If multiplex, efficiency and LOD of each assay.	<b>E</b>	N/A

**Table 4.** (Continued)

<b>DATA ANALYSIS</b>		
qPCR analysis program (source, version)	<b>E</b>	YES
Cq method determination	<b>E</b>	YES
Outlier identification and disposition	<b>E</b>	N/A
Results of NTCs	<b>E</b>	YES
Justification of number and choice of reference genes	<b>E</b>	YES
Description of normalisation method	<b>E</b>	YES
Number and concordance of biological replicates	<b>D</b>	YES
Number and stage (RT or qPCR) of technical replicates	<b>E</b>	YES
Repeatability (intra-assay variation)	<b>E</b>	YES
Reproducibility (inter-assay variation, %CV)	<b>D</b>	YES
Power analysis	<b>D</b>	NO
Statistical methods for result significance	<b>E</b>	YES
Software (source, version)	<b>E</b>	YES
Cq or raw data submission using RDML	<b>D</b>	N/A

### C. Phyre2 RESULTS

**Table 5.** Moh1p Phyre2 Results (Confidence > 80)

#	Template	Confidence	id %	Template Information
1	c8qbnY_	100	37	<b>PDB header:</b> ligase <b>Chain:</b> Y <b>PDB Molecule:</b> protein yippee-like 5 <b>PDBTitle:</b> structure of the non-canonical ctlh e3 substrate receptor wdr26 bound to ype15
2	c7sfzC_	96.9	22	<b>PDB header:</b> cell cycle <b>Chain:</b> C <b>PDB Molecule:</b> protein mis18-alpha <b>PDBTitle:</b> crystal structure of mis18a-yippee domain
3	c6uml C_	97.5	25	<b>PDB header:</b> ligase <b>Chain:</b> C <b>PDB Molecule:</b> protein cereblon <b>PDBTitle:</b> structural basis for thalidomide teratogenicity revealed by the2 cereblon-ddb1-sall 4-pomalidomide complex
4	c2k8dA_	90.7	20	<b>PDB header:</b> oxidoreductase <b>Chain:</b> A <b>PDB Molecule:</b> peptide methionine sulfoxide reductase msrb <b>PDBTitle:</b> solution structure of a zinc-binding methionine sulfoxide reductase

**Table 5.** (Continued)

<b>5</b>	c4v30A_	97.2	21	<b>PDB header:</b> signaling protein <b>Chain:</b> A <b>PDB Molecule:</b> cereblon isoform 4 <b>PDBTitle:</b> cereblon isoform 4 from magnetospirillum gryphiswaldense in complex2 with lenalidomide
<b>6</b>	c2l1uA_	88.3	17	<b>PDB header:</b> oxidoreductase <b>Chain:</b> A <b>PDB Molecule:</b> methionine-r-sulfoxide reductase b2, mitochondrial <b>PDBTitle:</b> structure-functional analysis of mammalian msrb2 protein
<b>7</b>	c6m6rA_	95.5	20	<b>PDB header:</b> rna binding protein/rna <b>Chain:</b> A <b>PDB Molecule:</b> dicer related helicase <b>PDBTitle:</b> crystal structure of caenorhabditis elegans dicer-related helicase 32 (drh-3) c-terminal domain with 5'-ppp 8-mer ssrna
<b>8</b>	c4a2vA_	88.9	18	<b>PDB header:</b> hydrolase <b>Chain:</b> A <b>PDB Molecule:</b> retinoic acid inducible protein i <b>PDBTitle:</b> structure of duck rig-i c-terminal domain (ctd)

**Table 5.** (Continued)

<b>9</b>	c3hcj B_	90.8	16	<b>PDB header:</b> oxidoreductase <b>Chain:</b> B <b>PDB Molecule:</b> peptide methionine sulfoxide reductase <b>PDBTitle:</b> structure of msrb from xanthomonas campestris (oxidized2 form)
<b>10</b>	c3ga3A_	95.5	19	<b>PDB header:</b> hydrolase <b>Chain:</b> A <b>PDB Molecule:</b> interferon-induced helicase c domain-containing protein 1 <b>PDBTitle:</b> crystal structure of the c-terminal domain of human mda5
<b>11</b>	c2w4rB_	95.1	16	<b>PDB header:</b> hydrolase <b>Chain:</b> B <b>PDB Molecule:</b> probable atp-dependent rna helicase dhx58; <b>PDBTitle:</b> crystal structure of the regulatory domain of human lgp2
<b>12</b>	c6symB_	89.6	16	<b>PDB header:</b> hydrolase <b>Chain:</b> G <b>PDB Molecule:</b> probable atp-dependent rna helicase ddx58; <b>PDBTitle:</b> crystal structure of the regulatory domain of human rig- i with bound2 zn
<b>13</b>	c2qfbG_	84.7	16	<b>PDB header:</b> hydrolase <b>Chain:</b> G <b>PDB Molecule:</b> probable atp-dependent rna helicase ddx58 <b>PDBTitle:</b> crystal structure of the regulatory domain of human rig- i with bound2 Zn

**Table 5.** (Continued)

<b>14</b>	c2kaoA_	91.6	22	<b>PDB header:</b> oxidoreductase <b>Chain:</b> A <b>PDB Molecule:</b> methionine-r-sulfoxide reductase b1 <b>PDBTitle:</b> structure of reduced mouse methionine sulfoxide reductase b12 (sec95cys mutant)
<b>15</b>	c6tr8A_	90.3	15	<b>PDB header:</b> oxidoreductase <b>Chain:</b> A <b>PDB Molecule:</b> peptide-methionine (r)-s-oxide reductase; <b>PDBTitle:</b> corynebacterium diphtheriae methionine sulfoxide reductase b (msrb)2 solution structure - reduced form
<b>16</b>	c5hj0C_	97.1	14	<b>PDB header:</b> ligase <b>Chain:</b> C <b>PDB Molecule:</b> kinetochore protein mis18 <b>PDBTitle:</b> crystal structure of mis18 'yippee-like' domain
<b>17</b>	c7e43A_	86.6	15	<b>PDB header:</b> oxidoreductase <b>Chain:</b> A <b>PDB Molecule:</b> peptide methionine sulfoxide reductase msra/msrb <b>PDBTitle:</b> structural insights into a bifunctional peptide methionine sulfoxide2 reductase msra/b fusion protein from helicobacter pylori

**Table 5.** (Continued)

<b>18</b>	c3cezA_	92.8	16	<b>PDB header:</b> oxidoreductase <b>Chain:</b> A <b>PDB Molecule:</b> methionine-r-sulfoxide reductase <b>PDBTitle:</b> crystal structure of methionine-r-sulfoxide reductase from2 burkholderia pseudomallei
<b>19</b>	c5fa9B_	91.8	13	<b>PDB header:</b> oxidoreductase <b>Chain:</b> B <b>PDB Molecule:</b> peptide methionine sulfoxide reductase msra <b>PDBTitle:</b> bifunctional methionine sulfoxide reductase ab (msrab) from treponema2 denticola
<b>20</b>	c3lrrB_	85.6	17	<b>PDB header:</b> hydrolase/rna <b>Chain:</b> B <b>PDB Molecule:</b> probable atp-dependent rna helicase ddx58 <b>PDBTitle:</b> crystal structure of human rig-i ctd bound to a 12 bp au rich 5' ppp2 dsrna
<b>21</b>	c6qa0A_	90.3	11	<b>PDB header:</b> oxidoreductase <b>Chain:</b> A <b>PDB Molecule:</b> methionine-r-sulfoxide reductase b3; <b>PDBTitle:</b> msrb3 - aa 1-137
<b>22</b>	c5e24D_	89.4	64	<b>PDB header:</b> transport/dna binding/dna <b>Chain:</b> D <b>PDB Molecule:</b> protein hairless; <b>PDBTitle:</b> structure of the su(h)-hairless-dna repressor complex
<b>23</b>	d1xm0a1	89.4	12	<b>Fold:</b> Mss4-like <b>Superfamily:</b> Mss4-like <b>Family:</b> Sel R domain

**Table 5.** (Continued)

<b>24</b>	d1l1da_	89.7	11	<b>Fold:</b> Mss4-like <b>Superfamily:</b> Mss4-like <b>Family:</b> Sel R domain
<b>25</b>	c7ctoF_	94	7	<b>PDB header:</b> oxidoreductase <b>Chain:</b> F <b>PDB Molecule:</b> peptide methionine sulfoxide reductase msrb <b>PDBTitle:</b> staphylococcus aureus msrb
<b>26</b>	c3e0mB_	93.3	7	<b>PDB header:</b> oxidoreductase <b>Chain:</b> B <b>PDB Molecule:</b> peptide methionine sulfoxide reductase msra/msrb 1 <b>PDBTitle:</b> crystal structure of fusion protein of msra and msrb

**Table 6.** YPEL2 Phyre2 Results (Confidence > 80)

#	Template	Confidence	id %	Template Information
1	c8qbnY_	100	45	<b>PDB header:</b> ligase <b>Chain:</b> Y <b>PDB Molecule:</b> protein yippee-like 5 <b>PDBTitle:</b> structure of the non-canonical ctlh e3 substrate receptor wdr26 bound2 to ypel 5
2	c2k8dA_	93.6	21	<b>PDB header:</b> oxidoreductase <b>Chain:</b> A <b>PDB Molecule:</b> peptide methionine sulfoxide reductase msrb <b>PDBTitle:</b> solution structure of a zinc-binding methionine sulfoxide reductase
3	c4v30A_	97.4	24	<b>PDB header:</b> signaling protein <b>Chain:</b> A <b>PDB Molecule:</b> cereblon isoform 4 <b>PDBTitle:</b> cereblon isoform 4 from magnetospirillum gryphiswaldense in complex2 with lenalidomide
4	c6umlC_	97.6	22	<b>PDB header:</b> ligase <b>Chain:</b> C <b>PDB Molecule:</b> protein cereblon <b>PDBTitle:</b> structural basis for thalidomide teratogenicity revealed by the2 cereblon-ddb1-sall 4-pomalidomide complex

**Table 6.** (Continued)

<b>5</b>	c2w4rB_	92.5	19	<p><b>PDB header:</b> hydrolase  <b>Chain:</b> B  <b>PDB Molecule:</b> probable atp-dependent rna helicase dhx58  <b>PDBTitle:</b> crystal structure of the regulatory domain of human lgp2</p>
<b>6</b>	c6qa0A_	94.1	18	<p><b>PDB header:</b> oxidoreductase  <b>Chain:</b> A  <b>PDB Molecule:</b> methionine-r-sulfoxide reductase b3  <b>PDBTitle:</b> msrb3 - aa 1-137</p>
<b>7</b>	c6tr8A_	93.9	21	<p><b>PDB header:</b> oxidoreductase  <b>Chain:</b> A  <b>PDB Molecule:</b> peptide-methionine (r)-s-oxide reductase  <b>PDBTitle:</b> corynebacterium diphtheriae methionine sulfoxide reductase b (msrb)2 solution structure - reduced form</p>
<b>8</b>	c3lrrB_	85.5	19	<p><b>PDB header:</b> hydrolase/rna  <b>Chain:</b> B  <b>PDB Molecule:</b> probable atp-dependent rna helicase ddx58  <b>PDBTitle:</b> crystal structure of human rig-i ctd bound to a 12 bp au rich 5' ppp2 dsrna</p>

**Table 6.** (Continued)

9	c6symB_	94	19	<p><b>PDB header:</b> oxidoreductase</p> <p><b>Chain:</b> B</p> <p><b>PDB Molecule:</b> peptide methionine sulfoxide reductase msrb</p> <p><b>PDBTitle:</b> crystal structure of escherichia coli msrb (reduced form)</p>
10	c4a2vA_	90	16	<p><b>PDB header:</b> hydrolase</p> <p><b>Chain:</b> A</p> <p><b>PDB Molecule:</b> retinoic acid inducible protein i</p> <p><b>PDBTitle:</b> structure of duck rig-i c-terminal domain (ctd)</p>
11	c6m6rA_	94.8	21	<p><b>PDB header:</b> rna binding protein/rna</p> <p><b>Chain:</b> A</p> <p><b>PDB Molecule:</b> dicer related helicase</p> <p><b>PDBTitle:</b> crystal structure of caenorhabditis elegans dicer-related helicase 32 (drh-3) c-terminal domain with 5'-ppp 8-mer ssrna</p>
12	c3hcjB_	93.2	15	<p><b>PDB header:</b> oxidoreductase</p> <p><b>Chain:</b> B</p> <p><b>PDB Molecule:</b> peptide methionine sulfoxide reductase</p> <p><b>PDBTitle:</b> structure of msrb from xanthomonas campestris (oxidized2 form)</p>
13	c7sfzC_	97	16	<p><b>PDB header:</b> cell cycle</p> <p><b>Chain:</b> C</p> <p><b>PDB Molecule:</b> protein mis18-alpha</p> <p><b>PDBTitle:</b> crystal structure of mis18a-yippee domain</p>

**Table 6.** (Continued)

<b>14</b>	c2qfbG_	88.6	15	<p><b>PDB header:</b> hydrolase  <b>Chain:</b> G  <b>PDB Molecule:</b> probable atp-dependent rna helicase ddx58  <b>PDBTitle:</b> crystal structure of the regulatory domain of human rig- i with bound Zn</p>
<b>15</b>	c5hj0C_	97.1	13	<p><b>PDB header:</b> ligase  <b>Chain:</b> C  <b>PDB Molecule:</b> kinetochore protein mis18  <b>PDBTitle:</b> crystal structure of mis18 'yippee-like' domain</p>
<b>16</b>	c5fa9B_	94.8	13	<p><b>PDB header:</b> oxidoreductase  <b>Chain:</b> B  <b>PDB Molecule:</b> peptide methionine sulfoxide reductase msra  <b>PDBTitle:</b> bifunctional methionine sulfoxide reductase ab (msrab) from treponema2 denticola</p>
<b>17</b>	c211uA_	92.1	15	<p><b>PDB header:</b> oxidoreductase  <b>Chain:</b> A  <b>PDB Molecule:</b> methionine-r-sulfoxide reductase b2, mitochondrial  <b>PDBTitle:</b> structure-functional analysis of mammalian msrb2 protein</p>
<b>18</b>	c2kaoA_	90.3	20	<p><b>PDB header:</b> oxidoreductase  <b>Chain:</b> A  <b>PDB Molecule:</b> methionine-r-sulfoxide reductase b1  <b>PDBTitle:</b> structure of reduced mouse methionine sulfoxide reductase b12 (sec95cys mutant)</p>

**Table 6.** (Continued)

<b>19</b>	c7ctoF_	95.3	12	<b>PDB header:</b> oxidoreductase <b>Chain:</b> F <b>PDB Molecule:</b> peptide methionine sulfoxide reductase msrb <b>PDBTitle:</b> staphylococcus aureus msrb
<b>20</b>	c3ga3A_	91	13	<b>PDB header:</b> hydrolase <b>Chain:</b> A <b>PDB Molecule:</b> interferon-induced helicase c domain-containing protein 1 <b>PDBTitle:</b> crystal structure of the c-terminal domain of human mda5
<b>21</b>	c3cezA_	94.7	14	<b>PDB header:</b> oxidoreductase <b>Chain:</b> A <b>PDB Molecule:</b> methionine-r-sulfoxide reductase <b>PDBTitle:</b> crystal structure of methionine-r-sulfoxide reductase from2 burkholderia pseudomallei
<b>22</b>	c3e0mB_	94.7	11	<b>PDB header:</b> oxidoreductase <b>Chain:</b> B <b>PDB Molecule:</b> peptide methionine sulfoxide reductase msra/msrb 1 <b>PDBTitle:</b> crystal structure of fusion protein of msra and msrb
<b>23</b>	d1xm0a1	92.3	12	<b>Fold:</b> Mss4-like <b>Superfamily:</b> Mss4-like <b>Family:</b> Sel R domain

**Table 6.** (Continued)

24	c7e43A_	92	12	<p><b>PDB header:</b> oxidoreductase  <b>Chain:</b> A  <b>PDB Molecule:</b> peptide methionine sulfoxide reductase msra/msrb  <b>PDBTitle:</b> structural insights into a bifunctional peptide methionine sulfoxide2 reductase msra/b fusion protein from helicobacter pylori</p>
25	c5e24D_	88.2	57	<p><b>PDB header:</b> transport/dna binding/dna  <b>Chain:</b> D  <b>PDB Molecule:</b> protein hairless;  <b>PDBTitle:</b> structure of the su(h)-hairless-dna repressor complex</p>
26	d111da_	94.3	8	<p><b>Fold:</b> Mss4-like  <b>Superfamily:</b> Mss4-like  <b>Family:</b> Sel R domain</p>

**D. SEM IMAGES OF LOGARITHMIC AND STATIONARY PHASE CELLS**

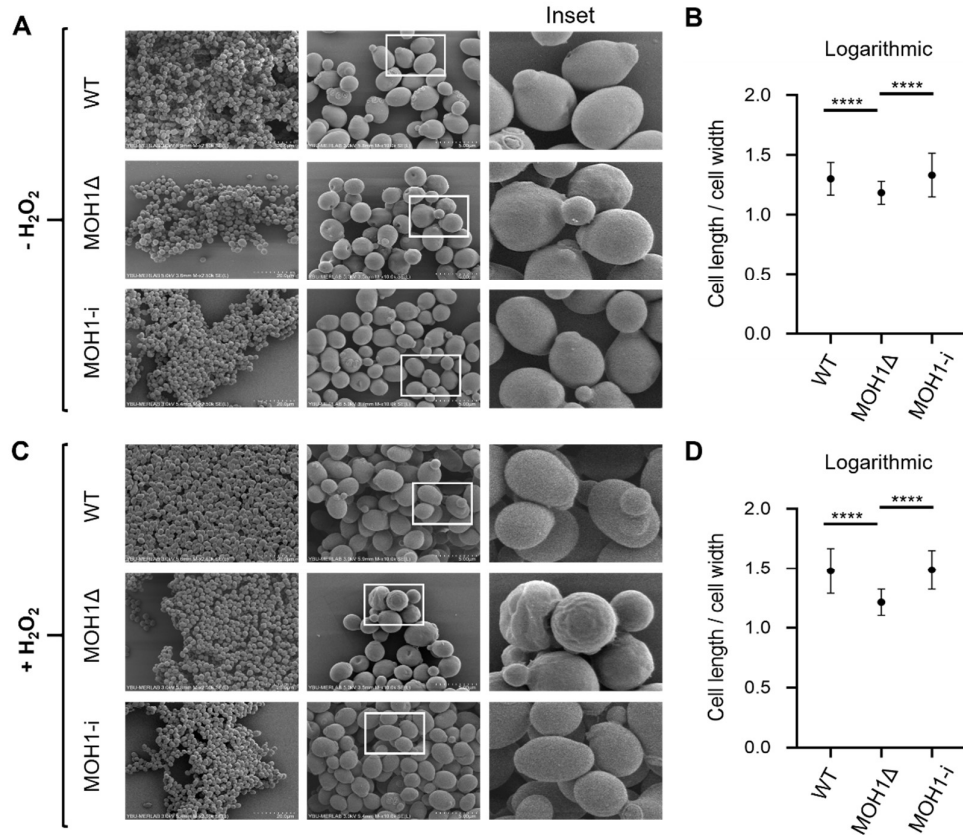


**Figure 13. SEM Images of WT, *moh1Δ*, and *moh1-i* cells at logarithmic phase in the presence and absence of  $H_2O_2$ .** A. SEM images in the absence of  $H_2O_2$ . White squares indicate Inset images. B. Cell length and width ratio in the absence of  $H_2O_2$ . C. SEM images in the presence of  $H_2O_2$ . White squares indicate Inset images. D. Cell length and width ratio in the presence of  $H_2O_2$ . Student t-test was conducted among groups for statistical difference. \*\*\*\* indicates significant difference ( $p < 0.001$ ).

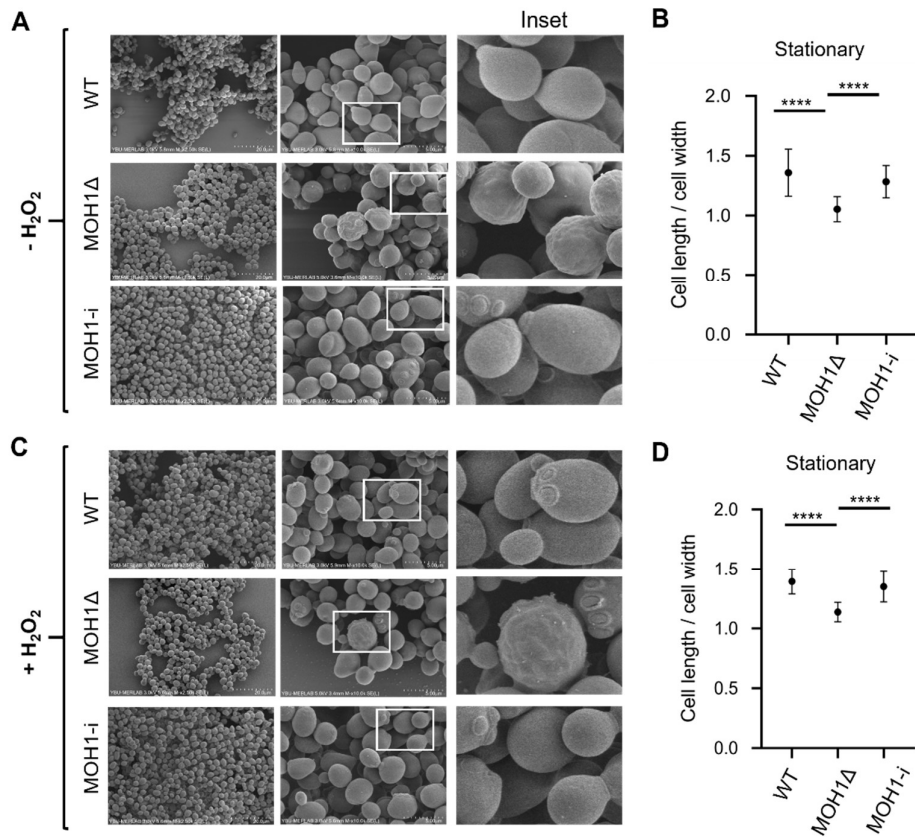


**Figure 14. SEM Images of WT, moh1Δ, and moh1-i cells at stationary phase in the presence and absence of stress. A.** SEM images in the absence of H<sub>2</sub>O<sub>2</sub>. White squares indicate Inset images. **B.** Cell length and width ratio in the absence of H<sub>2</sub>O<sub>2</sub> **C.** SEM images in the presence of H<sub>2</sub>O<sub>2</sub>. White squares indicate Inset images. **D.** Cell length and width ratio in the presence of H<sub>2</sub>O<sub>2</sub> **C.** Student t-test was conducted among groups for statistical difference. \*\*\*\* indicates significant difference ( $p < 0.001$ ).

## E. DIFFERENTIALLY EXPRESSED GENE LIST

**Table 7.** Differentially expressed genes when WT and moh1Δ cells compared

<b>Systematic Name</b>	<b>Gene Name</b>	<b>Log2 Fold Change</b>	<b>Adjusted p-value</b>
<b>YBL049W</b>	MOH1	-6,428332386	3,13E-58
<b>YCR018C-A</b>	YCR018C-A	-5,727669642	1,88E-54
<b>YMR323W</b>	ERR3	3,963633533	4,26E-19
<b>YBL048W</b>	RRT1	-2,662623772	2,37E-13
<b>YHR092C</b>	HXT4	1,777350656	1,02E-08
<b>YDL218W</b>	YDL218W	2,616126083	2,39E-06
<b>YDR034W-B</b>	CPP3	1,833289418	4,57E-06
<b>YNCJ0028C</b>	IRT1	1,494902813	5,74E-06
<b>YPL223C</b>	GRE1	1,22602174	2,20E-05
<b>YJR155W</b>	AAD10	1,56659673	2,38E-05
<b>YGR155W</b>	CYS4	1,029783629	0,000100923
<b>YKL221W</b>	MCH2	1,190305732	0,000241171
<b>YMR325W</b>	PAU19	3,571804424	0,000279455
<b>YGR087C</b>	PDC6	1,741279566	0,00036334
<b>YGL263W</b>	COS12	-2,17915759	0,000586242
<b>YMR032W</b>	HOF1	-1,240539441	0,000586242
<b>YAL023C</b>	PMT2	-1,065131943	0,000879719
<b>YOR247W</b>	SRL1	-1,516423755	0,001030188
<b>YHR214W-A</b>	YHR214W-A	-1,30193866	0,001486807
<b>YDL039C</b>	PRM7	2,072706193	0,002499803
<b>YMR324C</b>	YMR324C	3,930924205	0,003093842
<b>YJR094C</b>	IME1	1,545321287	0,004113023
<b>YDR297W</b>	SUR2	1,032835306	0,00463821
<b>YKL068W-A</b>	YKL068W-A	1,046620573	0,006810718
<b>YGL177W</b>	YGL177W	1,211506633	0,007194614
<b>YNCL0018W</b>	RDN5	-2,087843197	0,00935186
<b>YOR315W</b>	SFG1	-1,257929003	0,00935186
<b>YDR374C</b>	PHO92	2,12275328	0,01028738
<b>YER091C</b>	MET6	1,036596042	0,014045424
<b>YGR146C</b>	ECL1	1,185510434	0,015168998
<b>YGR144W</b>	THI4	1,311413389	0,017717567
<b>YLL067C</b>	YLL067C	-1,253496124	0,018082702
<b>YMR322C</b>	SNO4	1,329344536	0,02199161
<b>YJR115W</b>	YJR115W	1,177707103	0,026521778

**Table 7.** (Continued)

<b>Systematic Name</b>	<b>Gene Name</b>	<b>Log2 Fold Change</b>	<b>Adjusted p-value</b>
<b>YMR169C</b>	ALD3	1,265593012	0,028533969
<b>YPL281C</b>	ERR2	2,149782297	0,029049994
<b>YGR066C</b>	GID10	1,319162818	0,031497663
<b>YNL234W</b>	YNL234W	1,029735191	0,032005909
<b>YBR242W</b>	YBR242W	1,200320327	0,04198109
<b>YJR159W</b>	SOR1	1,250341501	0,04198109
<b>YDR048C</b>	YDR048C	4,88697742	0,04198109
<b>YGL158W</b>	RCK1	1,45846603	0,047126492
<b>YOL136C</b>	PFK27	1,267542807	0,047664313

## CURRICULUM VITAE

**Surname, Name:** Olgun, Çağla Ece

### EDUCATION

<b>Degree</b>	<b>Institution</b>	<b>Year of Graduation</b>
MSc	METU Molecular Biology and Genetics	2018
BS	METU Molecular Biology and Genetics	2015
High School	Süleyman Demirel Fen Lisesi, Edirne	2010

### WORK & RESEARCH EXPERIENCES

<b>Year</b>	<b>Place</b>	<b>Enrollment</b>
December, 2015 – Present	METU, Biological Sciences	Research Assistant
2014 June – August	German Center for Neurodegenerative Diseases (DZNE) within Helmholtz Association, Çağhan Kızıl's Lab	Intern Student
2011 June – August	Ankara University, Mustafa Akçelik's Lab	Intern Student

### PROJECTS

<b>Year</b>	<b>Name of the Project</b>	<b>Enrollment</b>
2014 November – July	Analysis of the Effect of the MOH1 Gene on Cell Morphology Through FT-IR Spectroscopy (TUBITAK, 124Z032)	Principle Investigator
2019 November – 2020 November	Functional characterization of human YPEL2 gene through its stress-responsive yeast homolog MOH1 by using transcriptomic analysis in yeast models (TUBITAK, 119Z570)	Principle Investigator

### FOREIGN LANGUAGES

Advanced English

## PUBLICATIONS

1. Turan G.\*, **Olgun Ç.E.\***, Ayten H., Toker P., Ashyrlayyev A., Savaş B., Karaca E., Muyan M. (2024). Dynamic proximity interaction profiling suggests that YPEL2 is involved in cellular stress surveillance. *Protein Science*. 33(2): e4859. doi: 10.1002/pro.4859 (\*first author)
2. Ayaz G.\*, Turan G.\*, **Olgun Ç.E.\***, Kars G., Karakaya B., Yavuz K., Demiralay Ö., Can T., Muyan M., Yaşar P. (2021). A prelude to the proximity interaction mapping of CXXC5. *Scientific Reports*. 11. doi: 10.1038/s41598-021-97060-6 (first author).
3. Ayaz G., Yaşar P., **Olgun Ç.E.**, Karakaya B., Kars G., Razizadeh N., Yavuz K., Turan G., Muyan M. (2019). Dynamic transcriptional events mediated by estrogen receptor alpha. *Frontiers in Bioscience*. 24, 245-276. doi: 10.2741/4716
4. **Olgun Ç.E.**, & Muyan M. (2018) SNW1 (SNW domain containing 1). *Atlas of Genetics and Cytogenetics in Oncology and Haematology*. 22(6):233-235. doi: 10.4267/2042/68909 (first author)